Coulomb Repulsion Effect in Two-electron Non-adiabatic Tunneling through a One-level redox Molecule

Medvedev, Igor M.; Kuznetsov, Alexander M.; Ulstrup, Jens

Published in:
Journal of Chemical Physics

Link to article, DOI:
10.1063/1.3253699

Publication date:
2009

Document Version
Publisher's PDF, also known as Version of record

Coulomb repulsion effect in two-electron nonadiabatic tunneling through a one-level redox molecule

Alexander M. Kuznetsov,[1] Igor G. Medvedev,[1,a)] and Jens Ulstrup[2]
[1]*A.N. Frumkin Institute of Physical Chemistry and Electrochemistry, Russian Academy of Sciences, Leninsky Prospect 31, Moscow 119991, Russian Federation*
[2]*Institute of Chemistry, Technical University of Denmark, Bldg. 207, DK-2800 Lyngby, Denmark*

(Received 31 July 2009; accepted 2 October 2009; published online 26 October 2009)

We investigated Coulomb repulsion effects in nonadiabatic (diabatic) two-electron tunneling through a redox molecule with a single electronic level in a symmetric electrochemical contact under ambient conditions, i.e., room temperature and condensed matter environment. The electrochemical contact is representative of electrochemical scanning tunneling microscopy or a pair of electrochemical nanoscale electrodes. The two-electron transfer molecular system also represents redox molecules with *three* electrochemically accessible oxidation states, rather than only *two* states such as comprehensively studied. It is shown that depending on the effective Coulomb repulsion energy, the current/overpotential relation at fixed bias voltage shows *two* narrow ($\sim k_B T$) peaks in the limit of strong electron-phonon coupling to the solvent environment. The system also displays current/bias voltage rectification. The differential conductance/bias voltage correlation can have up to four peaks even for a single-level redox molecule. The peak position, height, and width are determined by the oxidized and reduced states of both the ionization and affinity levels of the molecule and depend crucially on the Debye screening of the electric field in the tunneling gap. © *2009 American Institute of Physics*. [doi:10.1063/1.3253699]

I. INTRODUCTION

The study of electron tunneling through redox molecules in condensed matter environment at room temperature (*in situ* systems) is important in efforts toward new molecular scale electronics systems.[1–3] The notion "redox molecule" implies that the target bridge molecule has a single electrochemically accessible electronic level with two quasistable states. The electronic level is empty in one state (the oxidized state) and occupied in the other state (the reduced state). Strong interaction of the valence electrons with phonons in condensed matter environment is a crucial factor which distinguishes *in situ* systems from vacuum tunneling contacts. The theory of such systems was first considered in Ref. 4 and developed systematically in Refs. 5–13. Experimental studies of electron tunneling through redox molecules in electrochemical environment were initiated by Tao[14] and comprehensively extended in Refs. 15–20. It was shown in Refs. 4–7 that electron tunneling through the electronic states of the redox molecules is controlled by thermal fluctuations of the vibrational modes of the polar condensed media, resulting in a Frank–Condon factor in the transition probability expressions. Debye screening of the electric potential in the tunneling gap is another important feature[11,21] A crucial factor in the use of *in situ* electrochemical systems as molecular electronics elements is finally the option of independent variation of *two* potential drops: the bias voltage V between the enclosing electrodes and the electrochemical electrode potential φ (or overpotential η) of one of the electrodes relative to a third electrode (a reference electrode) equivalent to a gate voltage.[3] These two correlations correspond to the current/bias and the current/gate voltage correlations, respectively, of solid state single-molecule systems.[3]

Single-electron processes mediated by single-level redox molecules have mostly been in theoretical focus. This view accords with spinless models or infinitely large Coulomb repulsion U between two electrons occupying the same electronic energy level of the redox molecule. Even these simple systems display spectroscopic and transistorlike properties such as rectification, amplification, and negative differential conductance.[3,22] The tunneling current/overpotential and tunneling current/bias voltage dependences have been recorded and compared with theoretical predictions.[14,16–20] A particularly important observation is that the single-electron tunneling current/overpotential relation at fixed bias voltage, i.e., parallel variation of the electrochemical working electrode and tip potentials shows a maximum close to the electrochemical equilibrium potential of the redox molecule.[7,9,14,16–19]

Single-level redox molecules which can accept *two* or *more* electrons offer new properties.[23] Two- or multielectron transfer (multi-ET) are representative of electron tunneling through redox molecules with several, rather than only two electrochemically accessible oxidation states. Transition metal complexes based on Co, Ru, or Os, or on Mo and W may offer suitable molecular targets. Polynuclear transition metal complexes or even redox metalloproteins are other potential focus molecules. Metallic nanoparticles in the size range where room temperature single-electron charging is important (1.5–3 nm) is still another molecular scale multi-ET target system class.[24–26] Two-electron tunneling has

a)Electronic mail: theor@elchem.ac.ru.

been addressed for vacuum tunneling contacts (i.e., the electronic level of the bridge molecule fixed). It was shown that Coulomb blockade arises when the Coulomb repulsion energy U is much larger than both k_BT (where k_B is Boltzmann's constant and T the temperature) and the interaction of the bridge molecule with the electrodes but much smaller than accessible values of eV.[23,27–30] This leads to two steps in the current/bias voltage dependence. These are due to successive opening of new ET channels with increasing bias voltage associated with ET through the ionization and affinity levels of the bridge molecule[27–30] and correspond to two resonances in the differential conductance/bias voltage dependence.

Both Coulomb repulsion and electron-phonon interaction were taken into account in Refs. 31–33. Only the low-temperature limit (quantum phonon modes) and weak coupling with phonons were considered. The current/bias voltage dependence was found to show a steplike structure[32,33] with the electron-phonon coupling leading to small side bands in the differential conductance/bias voltage dependence.[31] The current/gate voltage dependence was not addressed. The linear differential conductance (at $V=0$) at low temperatures and in the presence of quantum phonon modes was analyzed in Ref. 34 using numerical renormalization group methods. It was shown that weak Coulomb blockade peaks in the conductance-gate voltage curves emerge for nonzero temperature or weak electron-phonon coupling. As in Refs. 27 and 29, these were correlated with the ionization and affinity levels of the bridge molecule.

In the present report we consider nonadiabatic (diabatic) tunneling (the limit of weak interaction of the redox molecule with the electrodes) of two electrons through the redox molecule. The weak-interaction limit is an important special case of electron tunneling. The ET process is of sequential character with intermediate electron localization in the valence orbital of the bridge molecule after configurational fluctuations and full vibrational relaxation. Renewed activation transmits the electron further, and the rate equation method can be used.[4,6,7,11,35–39]

We show that the interaction of both electrons with the same classical vibrational modes at room temperature ($k_BT=0.025$ eV) and the Coulomb repulsion U between the electrons located at the redox molecule result in a number of new effects: (1) the appearance of two peaks in the current/gate voltage dependence at arbitrary bias voltage. In contrast with observations in Ref. 34, the peaks are clear-cut, their widths are of the order of k_BT but with a different physical origin. The peaks appear when the average positions of the fluctuating ionization and affinity levels enter the energy window (energy gap) between the Fermi levels of the electrodes. The peaks are matched by Coulomb staircases in the tunneling current/bias voltage correlations and by other peaks in the differential conductivity/bias voltage correlation; (2) rectification in the current/bias voltage correlation determined by the effective Coulomb repulsion energy. (3) In contrast with previous observations, the differential conductance/bias voltage dependence can display up to four peaks related to the oxidized and reduced states of both ionization and affinity levels of the redox molecule. A short presentation of the results was given in two brief reports.[40,41] Presently we offer a more detailed treatment including proofs of main results. Particular attention is given to the different nature of the Coulomb blockade in the systems considered, i.e., condensed matter and vacuum tunneling contacts. For the sake of clarity the discussion is limited to symmetric (with respect to the electronic coupling of the molecule with the electrodes) tunneling contacts but this constraint can be relaxed straightforwardly. It is also shown that Debye screening is important and gives rectification and determines the differential conductance/bias voltage correlation.

The report is organized as follows. The model and the rate equations are given in Sec. II. The rate constants and reaction free energies are derived and discussed in Sec. III both for *in situ* and vacuum tunneling contacts. Some important tunneling current identities are also derived. The current/overpotential dependence is studied in Sec. IV based on approximate expressions for the tunneling current. Sec.V addresses rectification. The differential conductance is studied in Sec. VI. Some concluding remarks are offered in Sec. VII.

II. THE MODEL AND THE RATE EQUATIONS

The system Hamiltonian has the form:

$$H = H_{\mathrm{el}} + \frac{1}{2}\sum_k \hbar\omega_k(p_k^2 + q_k^2) \tag{1}$$

where H_{el} is the effective electronic Hamiltonian:

$$H_{\mathrm{el}} = \sum_{m\sigma} \varepsilon_m c_{m\sigma}^+ c_{m\sigma} + \sum_\sigma \left[\varepsilon_{\mathrm{b}}(q_k) n_\sigma + \frac{1}{2} U n_\sigma n_{-\sigma} \right] + \sum_{m\sigma} (V_m c_\sigma^+ c_{m\sigma} + V_m^* c_{m\sigma}^+ c_\sigma), \tag{2}$$

the subscript m on the right hand side of Eq. (2) runs through the values k or p, ε_k and ε_p being the electronic energies of the electrode quasiparticle states $|k\rangle$ and $|p\rangle$, respectively. σ is the spin projection, and $c_{m\sigma}^+$, $c_{m\sigma}$ the creation and annihilation operators for these states. $\varepsilon_{\mathrm{b}}(q_k)$ and $n_\sigma = c_\sigma^+ c_\sigma$ are the energy and occupation number operators of the valence orbital $|\mathrm{b}\rangle$ of the redox molecule. The third term on the right hand side of Eq. (2) describes the coupling between the electronic states of the electrodes and the bridge molecule with V_m as the coupling constants. The second term on the right hand side of Eq. (1) is the Hamiltonian of the phonon subsystem where p_k and q_k are the dimensionless momenta and coordinates of the solvent modes k which will be considered only in the classical limit; ω_k are the effective frequencies corresponding to the normal modes k. The electronic energy of the valence orbital then has the form

$$\varepsilon_{\mathrm{b}}(q_k) = \varepsilon_{\mathrm{b}} - \sum_k \gamma_k q_k. \tag{3}$$

ε_{b} is the energy of the valence level of the redox molecule when electron-phonon interaction is absent, counted from the Fermi level of the left electrode, and γ_k a set of coupling constants describing the interaction of the valence orbital of the redox molecule with the classical vibrational modes of

the condensed medium. ε_b incorporates the interaction of the valence electron with the electric field in the tunneling gap. ε_b and the Coulomb repulsion U also include the coupling of the ionic core of the redox molecule and its valence electrons to surface plasmons of the electrodes and the optical phonons of the polar environment (see, e.g., Ref. 42).

We consider the electronically weakly coupled tunneling limit when both conditions Δ, $k_BT_K \ll k_BT$ and $k_BT \ll E_r$ (or, more precisely,[12] Δ^L, $\Delta^R \ll (k_BTE_r)^{1/2}$) are valid. Kinetic master equations can then be used.[28,38] $\Delta=\Delta^L+\Delta^R$ is the total coupling strength of the valence level of the redox molecule with the left and right electrodes. Δ^L and Δ^R are defined as $\Delta^L=\pi\Sigma_k|V_k|^2\delta(\varepsilon-\varepsilon_k)$ and $\Delta^R=\pi\Sigma_p|V_p|^2\delta(\varepsilon-\varepsilon_p)$. Their physical meaning is that they are the half widths of the redox level appearing due to the coupling of this level with the left and right electrodes, respectively. We use the wide-band approximation for the electronic structures of the electrodes so that the parameters Δ^L and Δ^R are independent of energy. T_K is the Kondo temperature, and $E_r=0.5\Sigma_k\gamma_k^2/\hbar\omega_k$ the reorganization (Gibbs free) energy of the polar solvent (or the polaron shift energy). The redox molecule can have three charge states: uncharged (0), singly charged (1), and doubly charged (2). The probabilities of these states are denoted as P_0, $P_1=P_\sigma+P_{-\sigma}$, and P_2, where P_σ is the probability that the valence level is occupied by a single electron having spin projections σ, $P_\sigma=P_{-\sigma}$. Altogether, $P_0+P_1+P_2=1$. The rate equations are:

$$dP_0/dt = -2k_{01}P_0 + k_{10}P_1, \tag{4}$$

$$dP_\sigma/dt = k_{01}P_0 - k_{10}P_\sigma - k_{12}P_\sigma + k_{21}P_2, \tag{5}$$

$$dP_2/dt = -2k_{21}P_2 + k_{12}P_1, \tag{6}$$

where $k_{ij}=k_{ij}^L+k_{ij}^R$ are the rate constants for ET between the charge states i and j (i and $j=0,1,2$) which are the sum of the contributions from tunneling to or from the left and right electrodes. The probability of simultaneous two-electron transition is negligibly small in the weak tunneling limit because it is proportional to the second order of Δ and, moreover, has a four times larger Frank–Condon barrier than for single-ET. Using Eqs. (1)–(3), we obtain for the steady state,

$$P_0 = k_{10}k_{21}/Z, \quad P_1 = 2k_{01}k_{21}/Z, \quad P_2 = k_{01}k_{12}/Z, \tag{7}$$

$$j = 2e[k_{21}(k_{01}^Lk_{10}^R - k_{10}^Lk_{01}^R) + k_{01}(k_{12}^Lk_{21}^R - k_{21}^Lk_{12}^R)]/Z, \tag{8}$$

where $Z=k_{10}k_{21}+k_{01}(k_{12}+2k_{21})$. If P_2 is neglected (i.e., in the infinite U limit), Eqs. (1)–(8) coincide with the corresponding equations of Ref. 36. Since in many cases U is not only much larger than k_BT and Δ^L, Δ^R but also much larger than experimentally accessible values of $|eV|$ and $|e\eta|$, we study also the limit of infinite U. In this case

$$P_{0\infty} = k_{10}/Z_\infty, \quad P_{1\infty} = 2k_{01}/Z_\infty, \quad Z_\infty = 2k_{01} + k_{10}, \tag{9}$$

$$j_\infty = 2e(k_{01}^Lk_{10}^R - k_{10}^Lk_{01}^R)/Z_\infty. \tag{10}$$

Using the canonical transformation method (see the review article[2] and references therein) it can be shown that the electron tunneling through the single-level bridge molecule depends on the *effective* value $U_{eff}=U-2E_r$. A simple derivation of the expression for U_{eff} in nonadiabatic tunneling will be given in the next section. If $U_{eff}=0$, then $k_{01}=k_{12}$ and $k_{10}=k_{21}$ so that the tunneling current j_0 in this case is given by

$$j_0 = 2e(k_{01}^Lk_{10}^R - k_{10}^Lk_{01}^R)/(k_{01}+k_{10}). \tag{11}$$

It is obvious that j_0 is twice as large as in the spinless model [see, e.g., Eq. (1) of Ref. 13]. It should be noted that the tunneling current forms in the spinless model and in the model with the infinitely large Coulomb repulsion do not coincide.[10]

When U_{eff} takes large values for small V, and provided that $e\eta$ is of the same order as U_{eff}, the tunneling current due to the first ET to the redox molecule (which equals approximately j_∞) is much smaller then the tunneling current j_2 due to the second ET. Here

$$j_2 = 2e(k_{12}^Lk_{21}^R - k_{21}^Lk_{12}^R)/(k_{12}+2k_{21}). \tag{12}$$

As a result, $j \approx j_\infty + j_2$ for large U_{eff} and small V.

III. EXPRESSIONS FOR THE RATE CONSTANTS

As in the theory of nonadiabatic electrochemical ET,[43,44] the rate constants are calculated using Fermi's golden rule and can be written in the form

$$k_{ij}^\alpha = k^\alpha \int \frac{d\varepsilon}{2k_BT} f_\alpha(\varepsilon)\exp[-(E_r - \Delta F_{ji}^\alpha - \varepsilon + \varepsilon_F^\alpha)^2/4E_rk_BT], \tag{13}$$

for $j>i$ and

$$k_{ij}^\alpha = k_{ji}^\alpha \exp(-\Delta F_{ij}^\alpha/k_BT), \tag{14}$$

for $j<i$ where the detailed balance principle was used. α =L or R, $f_\alpha(\varepsilon)$ are the Fermi functions of the left and right electrodes with the Fermi energies ε_F^α, and ΔF_{ij}^α the reaction free energies for ET between the states i and j. The coefficients k^α are proportional to Δ^α. ΔF_{10}^L has the form[11]

$$\Delta F_{10}^L = \varepsilon_F^L - \varepsilon_B - \Delta F_{solv,10} - e[\varphi_L - \varphi_s] + e[\psi(z;\varphi_L - \varphi_L^{pzc}, \varphi_R - \varphi_R^{pzc}) - \varphi_s]. \tag{15}$$

The Fermi levels ε_F^L and ε_F^R are counted from the energies $-e\varphi_L$ and $-e\varphi_R$. φ_L and φ_R are the Galvani potentials of the left and right electrodes, respectively, and ε_B is the "bare" energy of the valence level of the redox molecule counted from the energy $-e\varphi_s$ where φ_s is the potential in bulk solution. $\Delta F_{solv,10}=-(Z-1)^2E_r+Z^2E_r=(2Z-1)E_r$ is the difference between the solvation free energies of the redox molecule in the reduced and oxidized states, Z is the charge of the bridge molecule having no valence electrons, and $\psi(z;\varphi_L - \varphi_L^{pzc}, \varphi_R - \varphi_R^{pzc})$ is the potential at the site z of the bridge molecule. This potential depends on the Galvani potentials φ_L and φ_R and on the potentials of zero charge φ_L^{pzc} and φ_R^{pzc} of the corresponding electrodes. It can be shown[11] that $\Delta F_{10}^R=\Delta F_{10}^L-eV$ where the bias voltage is defined as the difference of the electrochemical potentials of the left and right electrodes: $eV=\varepsilon_F^L-e\varphi_L-\varepsilon_F^R+e\varphi_R$.

We obtain for the free energy ΔF_{21}^{L}

$$\Delta F_{21}^{L} = \varepsilon_F^L - \varepsilon_B - \Delta F_{solv,21} - e[\varphi_L - \varphi_s] + e[\psi(z;\varphi_L - \varphi_L^{pzc}, \varphi_R - \varphi_R^{pzc}) - \varphi_s] - U, \quad (16)$$

where $\Delta F_{solcv,21} = -(Z-2)^2 E_r + (Z-1)^2 E_r = (2Z-3)E_r$. It follows from Eqs. (15) and (16) that

$$\Delta F_{21}^{L} = \Delta F_{10}^{L} - U_{eff}, \quad (17)$$

where

$$U_{eff} = U - \Delta F_{solv,10} + \Delta F_{solv,21} = U - 2E_r. \quad (18)$$

Equations (15) and (18) show that the energy of the singly occupied valence level and the Coulomb repulsion energy are shifted by $(2Z-1)E_r$ and $-2E_r$, respectively, due to the electron-phonon coupling. This result is a particular case of that given by Eqs. (5) and (6) of. Ref. 42. It is important that the shift of ε_B depends on Z. However, we put $Z=0$ in what follows. It should be noted that U_{eff} can also be negative (see, e.g., Ref. 45 and references therein).

As in Ref. 11, we introduce the "equilibrium" potentials φ_L^0 and φ_R^0 of the left and right electrodes, for the transfer of the first electron (i.e., the transition of the first electron to or from the redox molecule when $\varphi_L = \varphi_L^0$ and $V=0$ is in equilibrium at the left electrode so that $2k_{01}^{L} = k_{10}^{L}$). These potentials are determined by

$$\Delta F_{10}^{L} + k_B T \ln(2) = 0, \quad \Delta F_{10}^{R} + k_B T \ln(2) = 0. \quad (19)$$

The second terms on the left hand side of Eq. (19) incorporate the spin degeneracy of the Fermi levels in the metals. Using the "equilibrium" potential φ_L^0 we define the gate voltage as the "cathodic" overpotential $\eta = \varphi_L^0 - \varphi_L$. It can then be shown that[11]

$$\Delta F_{10}^{L} = e(\xi\eta + \gamma V) - k_B T \ln(2). \quad (20)$$

where $\xi(z) = 1 - \gamma(L-z, L_D) - \gamma(z, L_D)$; $\gamma(z) = \gamma(z, L_D)$, $\gamma(z, L_D) = \sinh(z/L_D)/\sinh(L/L_D)$. ξ and γ quantify the effect of the gate and bias voltage on the reaction free energies. The function $\gamma(z, L_D)$ depends on z/L and L_D/L where L is the width of the tunneling gap and L_D the Debye length. For example, $\gamma(z, L_D) \approx 0$ and $\gamma(z, L_D) \approx z/L$ for full $(L_D \ll L)$ and weak screening $(L_D \gg L)$, respectively. For the symmetric tunneling contact considered $k^L = k^R = k^0$ (the electrodes are made from the same metal) and $z = 0.5L$ so that $\xi = 1 - 2\gamma$ where $\gamma = \gamma(0.5L, L_D)$. The other reaction free energies are given by $\Delta F_{10}^{R} = e(\xi\eta + \gamma V) - eV - k_B T \ln(2)$, $\Delta F_{21}^{L} = e(\xi\eta + \gamma V) - k_B T \ln(2) - U_{eff}$, and $\Delta F_{21}^{R} = e(\xi\eta + \gamma V) - eV - k_B T \ln(2) - U_{eff}$.

The energy ε_b of the valence level of the redox molecule counted from the Fermi level of the left electrode is given by

$$\varepsilon_b = \varepsilon_B - \varepsilon_F^L + e[\varphi_L - \psi(z;\varphi_L - \varphi_L^{pzc}, \varphi_R - \varphi_R^{pzc})]. \quad (21)$$

It then follows from Eqs. (15) and (21) that $\varepsilon_b = -\Delta F_{10}^{L} - \Delta F_{solv,10}$ so that

$$\varepsilon_b = \varepsilon_b(q_k = 0) = -e(\xi\eta + \gamma V) + k_B T \ln(2) + E_r. \quad (22)$$

ε_b is thus the energy of the ionization level of the oxidized state of the redox molecule since this energy does not include the interaction with phonon modes. The last two terms on the right hand side of Eq. (22) appear due to the introduction of the equilibrium potential [see Eq. (10) of Ref. 11]. The affinity level energy is $\varepsilon_b + U_{eff}$. The energy of the singly occupied valence level of the reduced state of the redox molecule corresponding to full vibrational relaxation $\varepsilon_{b1} = \varepsilon_b(q_{k\alpha})$ is equal to $\varepsilon_b - 2E_r$ where $q_{k\alpha} = \gamma_k/\hbar\omega_k$ are the equilibrium values of the phonon coordinates.

The following electron-hole transformation of the Hamiltonian (1) gives an important tunneling current identity. We let $c_\sigma^+ \to b_\sigma$, $c_\sigma \to b_\sigma^+$, and $e \to -e$, where b_σ^+ and b_σ are creation and annihilation operators of the hole in the valence state of the redox molecule. The energy ε_{hole} of the singly occupied hole state counted from the Fermi level of the left electrode is then equal to $-\varepsilon_b - U$. In order to obtain the relation between the tunneling currents at $V>0$ and $V<0$, the difference between the equilibrium potentials for the transfer of the first electron and the first hole, respectively, from the left electrode to the redox molecule must be taken into account. It follows from Eq. (22) that $\varepsilon_b - k_B T \ln(2) - E_r = 0$ at $V=0$ and at the equilibrium potential φ_L^0. An analogous equation is valid for ε_{hole} at $V=0$ and at the equilibrium potential $(\varphi_L^0)_{hole}$ for transfer of the first hole to the valence state of the redox molecule: $\varepsilon_{hole} - k_B T \ln(2) + 3E_r = -\varepsilon_b - U - k_B T \ln(2) + 3E_r = 0$, where $3E_r$ is the solvation free energy difference of the redox molecule after transfer of a hole to the valence orbital initially occupied by two electrons. When $\varphi_L = (\varphi_L^0)_{hole}$, the energy $e\xi\eta$ is therefore equal to $U_{eff} + 2k_B T \ln(2)$, Eq. (22). As a result, we obtain the identity

$$j(V, e\xi\eta, U_{eff}) = -j(-V, -e\xi\eta + U_{eff} + 2k_B T \ln(2), U_{eff}). \quad (23)$$

valid for nonsymmetric contacts as well. Equation (23) can also be obtained directly from Eqs. (13) and (14).

Concluding this section we consider the rate constants for a vacuum tunneling contact. Equations (13) and (14) can still be used if valence electrons of the bridge molecule are coupled to the classical intramolecular vibrations (we neglect here coupling of the valence electron with high-frequency intramolecular quantum modes). For electrodes made of the same metals,

$$\Delta F_{10}^{L} = -\varepsilon_{b0} + \gamma eV, \quad (24)$$

where

$$\varepsilon_{b0} = \varepsilon_B - \varepsilon_F^L + e(\varphi_L^{pzc} - \varphi_{vac}) - E_r \quad (25)$$

is the bare electronic energy counted from the Fermi level of the left electrode at the potential of zero charge including the interaction of the valence electron with intramolecular vibrations. The energy of the singly occupied valence level ε_{b1} thus equals $\varepsilon_{b0} - e\gamma V$, E_r is the reorganization energy and $\gamma = z/L$ for vacuum tunneling contacts where Debye screening is absent. In order to compare the results for vacuum and *in situ* tunneling, it is convenient to introduce "the overpotential" η_0 defined as $e\eta_0 = -\varepsilon_{b0} + k_B T \ln(2)$ so that $\Delta F_{10}^{L} = e(\eta_0 + \gamma V) - k_B T \ln(2)$.

If coupling between valence electrons and intramolecular modes is absent, the rate constants can also be obtained

from Eq. (13) in the limit $E_r \to 0$. Since $\beta \exp[-(\beta x)^2]/\pi^{1/2}$ tends to the delta-function $\delta(x)$ when $\beta \to \infty$, we obtain

$$k_{ij}^{\alpha} = C^0 \exp(\Delta F_{ji}^{\alpha}/k_B T)/[1+\exp(\Delta F_{ji}^{\alpha}/k_B T)], \quad (26)$$

for $j > i$, and

$$k_{ij}^{\alpha} = C^0/[1+\exp(\Delta F_{ij}^{\alpha}/k_B T)]; \quad C^0 = k^0(\pi E_r/k_B T)^{1/2}, \quad (27)$$

for $j < i$. As k^0 is proportional to $1/E_r^{1/2}$,[43] the coefficient C^0 is independent of E_r.

For arbitrary E_r and the vacuum tunneling contact,

$$(\varepsilon_{b0})_{hole} = -\varepsilon_B - U + \varepsilon_F^L - e(\varphi_L^{pzc} - \varphi_{vac}) + 3E_r = -\varepsilon_{b0} - U_{eff}. \quad (28)$$

Therefore, $(e\eta_0)_{hole} = \varepsilon_{b0} + U_{eff} + k_B T \ln(2) = -e\eta_0 + U_{eff} + 2k_B T \ln(2)$ so that identity (23) applies but in the slightly different form:

$$j(V, e\eta_0, U_{eff}) = -j(-V, -e\eta_0 + U_{eff} + 2k_B T \ln(2), U_{eff}), \quad (29)$$

where $U_{eff} = U$ when $E_r = 0$.

Another identity for the tunneling current, valid only for a symmetric vacuum tunneling contact ($z = 0.5L$, $\gamma = 0.5$) can be obtained. The difference between the singly occupied valence level of the redox molecule and the Fermi level of the left electrode, $\varepsilon_{bL}(V)$, equals $\varepsilon_{b0} - \gamma eV$. The difference of this level from the Fermi level of the right electrode, $\varepsilon_{bR}(V)$, is $\varepsilon_{b0} + (1-\gamma)eV$. We then obtain that $\varepsilon_{bL}(V) = \varepsilon_{bR}(-V)$ for $\gamma = 0.5$. Since the electrodes are made of the same metal,

$$j(V, e\eta_0, U_{eff}) = -j(-V, e\eta_0, U_{eff}). \quad (30)$$

Equation (30) shows that, at given η_0 and $\gamma = 0.5$, the tunneling current is an odd function of V so that rectification is impossible for the symmetric vacuum contact. Also from Eqs. (29) and (30),

$$j(V, e\eta_0, U_{eff}) = j(V, -e\eta_0 + U_{eff} + 2k_B T \ln(2), U_{eff}). \quad (31)$$

The tunneling current is here an even function of η_0 when $U_{eff} = -2k_B T \ln(2)$.

IV. APPROXIMATE PROBABILITY AND TUNNELING CURRENT EXPRESSIONS: THE TUNNELING CURRENT/OVERPOTENTIAL DEPENDENCE

In this section we derive approximate expressions for the tunneling current and the tunneling current/overpotential dependencies. The effective overpotentials,

$$\eta_V = \xi\eta + (\gamma - 1/2)V, \quad \eta_{0V} = \eta_0 + (\gamma - 1/2)V, \quad (32)$$

are useful for the analysis of the current/overpotential dependence.[9] We start from the pure vacuum tunneling contact when $E_r = 0$. From Eqs. (9), (10), and (25)–(27), in the infinite-U limit

$$P_{0\infty,vac} = [\exp(-e\eta_{0V}/2k_B T) + \cosh(eV/2k_B T)]/Z_{\infty,vac}, \quad (33)$$

$$P_{1\infty,vac} = 1 - P_{0\infty,vac},$$

$$j_{\infty,vac} = 2eC^0 \sinh(eV/2k_B T)/Z_{\infty,vac}, \quad (34)$$

$$Z_{\infty,vac} = 2^{3/2} \cosh[(e\eta_{0V} - 0.5k_B T \ln(2))/k_B T] + 3\cosh(eV/2k_B T). \quad (35)$$

The tunneling current/overpotential dependence in the infinite-U limit and $\gamma = 0.5$ has a maximum at $(e\eta_0)_{max} = (\varepsilon_{b0})_{max} = k_B T \ln(2)/2$, Eqs. (34) and (35) so that the ionization level $(\varepsilon_{b1})_{max} = (\varepsilon_{b0})_{max} - 0.5eV$ is approximately at the center of the energy window. The width $W_{\infty,vac}$ of the current/overpotential curve at half maximum is given by

$$W_{\infty,vac} = 2k_B T \ln\{\text{arccosh}[2 + 3\cosh(eV/2k_B T)/2^{3/2}]\}. \quad (36)$$

The width increases monotonically from $eW_{\infty,vac} \approx 4k_B T$ for $eV \ll 2k_B T$ to $eW_{\infty,vac} \approx eV$ for $eV \gg 2k_B T$. This result is obvious since for $eV \gg 2k_B T$ the tunneling current takes rather large values [no smaller than $j_{\infty,vac}((e\eta_0)_{max})/2$] when ε_{b0} lies in the energy window and varies from 0 to eV.

Using Eq. (12) the tunneling current $j_{2,vac}$ is found to have the same form as $j_{\infty,vac}$ and differs from the latter only by the argument of the first cosh on the right hand side of Eq. (35):

$$j_{2,vac} = 2eC^0 \sinh(eV/2k_B T)/Z_{2,vac}, \quad (37)$$

$$Z_{2,vac} = 2^{3/2} \cosh[(e\eta_{0V} - U - 3k_B T \ln(2)/2)/k_B T] + 3\cosh(eV/2k_B T). \quad (38)$$

As a result, the tunneling current $j_{2,vac}$ assumes a maximum at $(e\eta_0)_{max} = U + 3k_B T \ln(2)/2$ [or $(\varepsilon_{b0})_{max} + U = -k_B T \ln(2)/2$] so that the affinity level $(\varepsilon_{bL}(V))_{max} + U = (\varepsilon_{b0})_{max} - 0.5eV + U$ is approximately at the center of the energy window. The $j_{2,vac}(\eta_0)$ curve has the same width at half maximum as the $j_{\infty,vac}(\eta_0)$ curve. Figure 1 shows current/overpotential dependencies for the vacuum tunneling contact. Since $j_{vac} \approx j_\infty + j_2$ at small V and large U, a clear peak is observed; Fig. 1(a) with the Coulomb blockade peak at $e\eta_0 \approx U$.

As noted in Sec. II, the overlap between the peaks increases with increasing V or decreasing U, and merge into a single peak, Fig. 1(b) at a critical value $U_{*,vac}$, which depends on V. This value can be roughly estimated as $eW_{\infty,vac}/2$ so that $U_{*,vac} \approx 2k_B T$ for $eV \ll 2k_B T$ and $U_{*,vac} \approx eV/2$ for $eV \gg 2k_B T$. It follows from Eqs. (34) and (35) that $j_{\infty,vac} \to \pm 2eC^0/3$ when $|V| \to \infty$. Using Eqs. (8), (26), and (27) the total tunneling current j_{vac} is found to tend to $\pm eC^0$, when $|V| \to \infty$, giving for the ratio $j_{\infty,vac}/(j_{vac} - j_{\infty,vac}) = 2$.[30]

When the interaction of the valence electron with classical environmental and the classical intramolecular phonon modes in the case of the vacuum tunneling contact is strong ($E_r > 0$), several useful approximate tunneling current expressions apply in the large-E_r limit ($|\Delta F_{ij}^{\alpha}| \ll E_r$) both for vacuum and the *in situ* tunneling. We shall use the variables η_V and $\xi\eta$ in all expressions below. These should be replaced by η_{0V} and η_0 for the vacuum tunneling contact. Only the linear ΔF_{ij}^{α} term is retained in the quadratic free energy form on the right hand side of Eq. (13) in this limit. Equation (13) then reduces to[43]

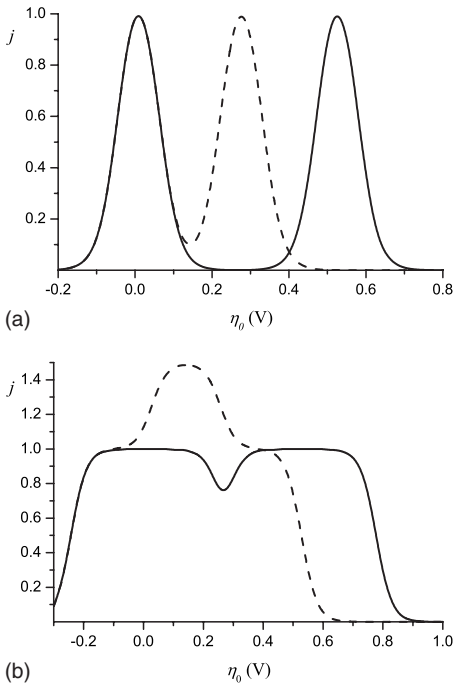

FIG. 1. Dependence of the tunneling current on the "overpotential" for the vacuum tunneling contact (E_r=0). The current j is normalized to the tunneling current j_∞ for infinitely large Coulomb repulsion energy at $(e\eta_0)_{max}=k_BT\ln(2)/2$. γ=0.5, k_BT=0.025 eV. Solid line: U=0.5 eV. Dashed line: U=0.25 eV. (a) V=0.1 V. (b) V=0.5 V.

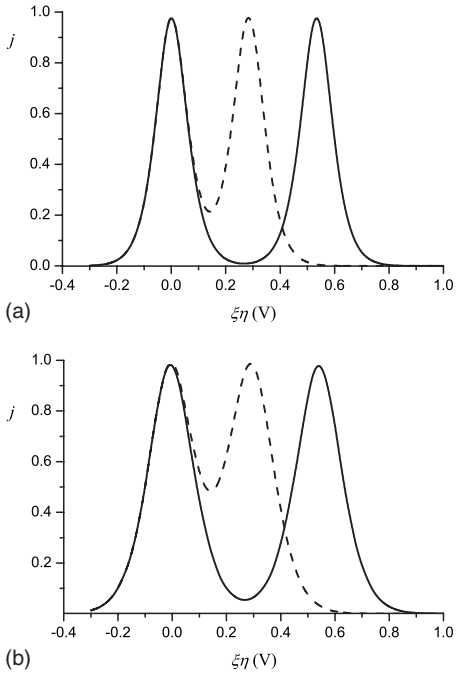

FIG. 2. Dependence of the tunneling current on the overpotential. Condensed matter *in situ* environment. Large positive U_{eff}. The current j is normalized to the tunneling current $j_\infty(0)$ for infinitely large Coulomb repulsion energy at zero effective overpotential. E_r=0.5 eV, γ=0.2, and k_BT=0.025 eV. Solid line: U_{eff}=0.5 eV. Dashed line: U_{eff}=0.25 eV. (a) V=0.1 V; (b) V=0.5 V.

$$k_{ij}^{\alpha}=k^{\alpha}(\pi/2)\exp(-E_r/4k_BT)\exp(\Delta F_{ji}^{\alpha}/2k_BT). \tag{39}$$

Using Eqs. (7), (8), (14), and (39),

$$P_0=1/Z_P,\quad P_1=\exp(e\eta_V/k_BT)/Z_P,$$
$$P_2=0.25\exp[(2e\eta_V-U_{eff})/k_BT]/Z_P, \tag{40}$$

where

$$Z_P=1+\exp(e\eta_V/k_BT)+0.25\exp[(2e\eta_V-U_{eff})/k_BT)], \tag{41}$$

and

$$j=2\pi ek^0 2^{1/2}\exp(-E_r/4k_BT)\times\frac{\sinh(eV/4k_BT)\{2+\exp[(2e\eta_V-U_{eff})/2k_BT]\}}{8\cosh(e\eta_V/2k_BT)+\exp[(3e\eta_V-2U_{eff})/2k_BT]}. \tag{42}$$

The tunneling current j_∞ can be obtained from Eq. (10) or Eq. (42) in the limit $U_{eff}\gg|e\eta_V|$, k_BT. This expression is the symmetric special case of Eq. (A3) in Ref. 11 and has the simple form:

$$j_\infty=\pi ek^0 2^{1/2}\exp(-E_r/4k_BT)\frac{\sinh(eV/4k_BT)}{2\cosh(e\eta_V/2k_BT)}. \tag{43}$$

Equation (43) shows that in the infinite-U_{eff} limit the current/overpotential dependence has a maximum at η_V=0 [or $\xi\eta=(0.5-\gamma)V$].[11] It also follows from Eq. (43) that, in the large E_r limit, $j_\infty(V,\eta)=-j_\infty(-V,-\eta)$. We obtain from Eqs. (40) and (41) that $P_{0\infty}=1/[1+\exp(e\eta_V/k_BT)]$ and $P_{1\infty-}=1-P_{0\infty}$.

The expression for the tunneling current j_2 can also be obtained directly using Eq. (12) or Eq. (42) in the limit when U_{eff} is of the order of $|e\eta_V|$ and $U_{eff}\gg k_BT$, giving

$$j_2=\pi ek^0 2^{1/2}\exp(-E_r/4k_BT)\times\frac{\sinh(eV/4k_BT)}{2\cosh[e\eta_V-U_{eff}-2k_BT\ln(2)]/2k_BT)}. \tag{44}$$

The current/overpotential dependence represented by Eq. (44) is maximum at $e\eta_V=U_{eff}+2k_BT\ln(2)$ [or at $e\xi\eta=(0.5-\gamma)V+U_{eff}+2k_BT\ln(2)$].

As for pure vacuum tunneling, the total tunneling current j at large U and small V, equals approximately $j_\infty+j_2$ so that the first current/overpotential peak is associated with the current j_∞ and the Coulomb blockade peak with $j_{2,vac}$, Fig. 2. Both peaks have the same height and width. Equations (43) and (44) show that the peak width W is $4k_BT\ln(2+3^{1/2})\approx 5.2k_BT\approx 0.13$ eV and independent of E_r and V in the large-E_r limit. The important difference between pure vacuum and *in situ* tunneling or vacuum tunneling with electron-phonon interaction is the existence of the new energy parameter (the reorganization energy) which can be large. The energy $e\eta_V$ has a single energy scale k_BT in this case, Eqs. (43) and (44). In contrast with pure vacuum tunneling, W is therefore of the order of k_BT even for eV of the order of E_r so that both peaks are clear-cut [compare Figs. 1(b) and 2(b)]. The origin of this difference is the different forms of the density of the electronic states at the valence orbital of the bridge molecule (or the spectral function). The density of states is delta-function-like for pure vacuum tunneling. The total density of states in the infinite-U limit for

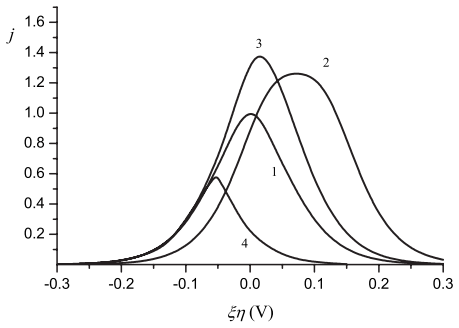

FIG. 3. Dependence of the tunneling current on the overpotential. Either positive or negative, small U_{eff}. The current j is normalized to $j_\infty(0)$ where $j_\infty(0)$ is the tunneling current for infinitely large Coulomb repulsion energy at zero value of the effective overpotential E_r=0.5 eV, γ=0.2, V=0.1 V, k_BT=0.025 eV. (1) $U=\infty$. (2) U_{eff}=0.05 eV. (3) U_{eff}=0. (4) U_{eff}=−0.15 eV.

the *in situ* systems or vacuum tunneling contacts with electron-phonon interaction is the sum of the density of the oxidized states centered at ε_b and the density of the reduced states centered at ε_b-2E_r.[12,13] The width at half maximum is $4(E_rk_BT)^{1/2}$ for both densities of states. It can be shown that the behavior of these densities of states near the center of the energy window is determined by the ratio $e\eta_V/k_BT$ in the large-E_r limit.

From Eq. (22), $\varepsilon_b=-e\eta_V-eV/2+k_BT\ln(2)+E_r$ in terms of the effective overpotential. The first and the second peaks of the current/overpotential dependence are therefore located at values of η_V, which correspond to the case when the thermally fluctuating ionization or affinity levels $\varepsilon_b(q_{k\alpha}/2)=-e\eta_V-eV/2+k_BT\ln(2)$ or $\varepsilon_b(q_{k\alpha}/2)+U_{\text{eff}}$ (but not their fixed positions as in the absence of electron-phonon coupling) are approximately at the center of the energy window. It is obvious that Eq. (23) correlates the tunneling current at the first peak at $V>0$ with those at the Coulomb blockade peak at $V<0$. When U_{eff} decreases, the peaks begin to overlap, merging into a single peak at $U_{\text{eff}}<U_{\text{eff}^*}$. U_{eff^*} can be estimated as $W/2\approx 2.6k_BT$. A similar result is demonstrated by Fig. 1c of Ref. 30, which shows the merging of peaks at $U_{\text{eff}}\approx 2k_BT$ for the vacuum tunneling contact at low temperatures and coupling to quantum phonon modes.

We so far discussed the current/overpotential dependence based on the approximate expression $j\approx j_\infty+j_2$. A more rigorous way is to use of Eq. (42). Using Eq. (42), it is shown in Appendix A that there are two peaks in the current/overpotential correlation for $U_{\text{eff}}>U_{\text{eff}^*}=2k_BT\ln(3)\approx 0.055$ eV at fixed bias voltage. The peaks are located at $e\eta_V\approx 0$ and $e\eta_V\approx U_{\text{eff}}+2k_BT\ln(2)$ as obtained above using the approximate expression. The minimum of the $j(\eta_V)$ curve is at $e\eta_V=U_{\text{eff}}/2+k_BT\ln(2)$. The peaks merge into a single peak at $U_{\text{eff}}<U_{\text{eff}^*}$ with the maximum of the resulting curve at $e\eta_V=U_{\text{eff}}/2+k_BT\ln(2)$ both for positive and negative U_{eff} (see Fig. 3). These results apply to the large-E_r limit.

In order to study the case when $U_{\text{eff}}<U_{\text{eff}^*}$, we rewrite Eq. (42) in the form

$$j=2\pi ek^0\exp(-E_r/4k_BT)\sinh(eV/4k_BT)\times\exp(U_{\text{eff}}/4k_BT)\frac{\cosh(D/2k_BT)}{\cosh(D/k_BT)+\exp(U_{\text{eff}}/2k_BT)},\tag{45}$$

where $D=e\eta_V-U_{\text{eff}}/2-k_BT\ln(2)$. Equation (45) shows that the current/overpotential extremum is at the point $e\eta_V=U_{\text{eff}}/2+k_BT\ln(2)$. When $U_{\text{eff}}=0$, Eq. (45) takes the simple form:

$$j_0=\pi ek^0\exp(-E_r/4k_BT)\frac{\sinh(eV/4k_BT)}{\cosh[(e\eta_V-k_BT\ln(2))/2k_BT]}.\tag{46}$$

As a result, the maximum value of j_0 exceeds the maximum value of j_∞ by $2^{1/2}$.

When $U_{\text{eff}}<0$ and $|U_{\text{eff}}|\gg k_BT$, Eq. (45) takes the form

$$j=2\pi ek^0\exp(-E_r/4k_BT)\sinh(eV/4k_BT)\times\exp(U_{\text{eff}}/4k_BT)\frac{\cosh(D/2k_BT)}{2\cosh^2(D/2k_BT)-1}.\tag{47}$$

The maximum tunneling current in the current/gate voltage dependence is thus proportional to $\exp(-|U_{\text{eff}}|)$ and is rather small (see Fig. 3).

Figures 1–3 show that the single-level bridge molecule system can operate as an amplifier with two regions of amplification for large U_{eff} but only a single region when $U_{\text{eff}}<U_{\text{eff}^*}$. In the latter case the amplification is largest when $U_{\text{eff}}=0$, Eq. (45).

In the small-E_r limit ($|\Delta F_{ij}^{\alpha}|\gg E_r$) the expressions for $P_{i\infty}$, j_∞, and j_2 coincide with those given by Eqs. (33)–(35), (37), and (38) for vacuum tunneling, with $\xi\eta$ substituted for η_0 and U_{eff} for U, Appendix B. The peak positions of the current/overpotential curves are therefore almost the same in the limits of large and small E_r and differ only by terms of the order of k_BT. It follows from these expressions as well as from the results in Appendix B that $P_{0\infty}=1/3$, $P_{1\infty}=2/3$, and $|j_\infty|=2ek^0(\pi E_r/k_BT)^{1/2}/3$ in the limit $U_{\text{eff}}\gg|V|\to\infty$. It also follows from Appendix B that the total probabilities P_i and the total tunneling current $P_0=P_2\approx 1/4$, $P_1=1/2$, and $|j|=ek^0(\pi E_r/k_BT)^{1/2}$, as $|V|\to\infty$. As for vacuum tunneling,[30] the current/bias voltage dependence for the *in situ* symmetric tunneling contact and large U_{eff} therefore has two steps where the first step is twice as large as the second one. This is due to the common physical nature of this phenomenon which is independent of the type of the tunneling contact, namely, the empty ionization level of the redox molecule can accept an electron with two different spin projections whereas the spin of the second electron transferred to the affinity level must be opposite to the spin of the first one.[30]

V. RECTIFICATION

Rectification is usually associated with two-quantum dot systems[46–49] or a single-level bridge molecule in asymmetric tunneling contacts.[49,50] Equation (30) shows that rectification is impossible for symmetric vacuum tunneling contacts even when electron-phonon interactions are included. However, in

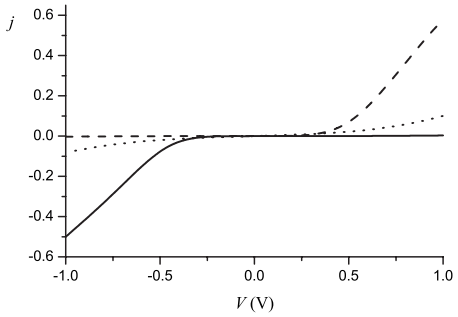

FIG. 4. Dependence of the tunneling current on the bias voltage for $U=\infty$ to illustrate rectification. The current is normalized to $4ek^0$. $E_r=0.5$ eV, $\gamma=0.2$, and $k_BT=0.025$ eV. Dotted line: $\eta=0$. Dashed line: $\xi\eta=0.2$ V. Solid line: $\xi\eta=-0.2$ V.

the present section we show that rectification emerges for *in situ* symmetric tunneling contacts when Debye screening is taken into account, cf. Ref. 21. The parameter γ is then $\gamma(0.5L,L_D)=\sinh(0.5L/L_D)/\sinh(L/L_D)=0.5/\cosh(0.5L/L_D)$ and varies from ≈ 0 for strong screening to ≈ 0.5 for weak screening. We consider intermediate screening. For the sake of specific illustration we assume that $\gamma=0.2$ (corresponding to $L_D/L=0.32$). We start from the infinite-U limit and show that rectification is expected already in this limit. In addition we assume that $4k_BT \ll (1-2\gamma)e|V|$, $e|\xi\eta+(\gamma-0.5)V| \ll E_r$, and $|\eta| \ll |V|$. These conditions are satisfied, e.g., for 0.5 V $<|V|<1$ V and $|\eta|<0.5$ V. In this experimentally important region of V and η, the following approximate current expression applies, Eq. (43):

$$j_\infty(V,\eta) \approx j_{\infty,\mathrm{appr}}(V,\eta) = \pm 2^{-1/2} e\pi k^0 \exp(-E_r/4k_BT) \times \exp[\pm e(\xi\eta+\gamma V)/2k_BT]. \quad (48)$$

The signs (+) and (−) on the right hand side of Eq. (48) correspond to $V>0$ and $V<0$, respectively.

Equation (48) shows that rectification is expected in the infinite-U limit when $\eta \neq 0$ since the rectification ratio $r(V,\xi\eta)$ defined as $r(V,\xi\eta)=j_\infty(|V|,\xi\eta)/|j_\infty(-|V|,\xi\eta)|$ is proportional to $\exp(e\xi\eta/k_BT)$. Equation (48) also shows that the tunneling current is suppressed in the region $V<0$ ($V>0$) for $\eta>0$ ($\eta<0$) and vice versa, Fig. 4. For example, $r(0.5\text{ V},-0.2\text{ V})=210$ and $r(1\text{ V},-0.2\text{ V})=150$. Rectification, however, only appears when $e|\xi\eta+(\gamma-0.5)V| \ll E_r$. The absolute tunneling current values thus tend to their asymptotic value $2ek^0(\pi E_r/k_BT)^{1/2}/3$, which is the same for $V>0$ and $V<0$ when $|V| \gg E_r$. The physical nature of the rectification is discussed in Sec. VI. Figure 4 also shows that the identity $j_\infty(V,\eta)=-j_\infty(-V,-\eta)$ is valid in the large-E_r limit.

We consider next finite U_{eff}. We assume that all the inequalities for V and η above remain valid and that $|U_{\mathrm{eff}}| < |(0.5-\gamma)eV|$, $|U_{\mathrm{eff}}| \gg k_BT$. It then follows from Eqs. (42) and (48) that $j(V,\xi\eta,U_{\mathrm{eff}}) \approx j_\infty(V,\xi\eta)$ for $V>0$ and

$$j(V,\xi\eta,U_{\mathrm{eff}}) \approx 2j_{\infty,\mathrm{appr}}(V,\xi\eta)\exp(U_{\mathrm{eff}}/2k_BT), \quad (49)$$

for $V<0$. In particular, $j(V,\xi\eta,U_{\mathrm{eff}})=2j_{\infty,\mathrm{appr}}(V,\xi\eta)$ at $U_{\mathrm{eff}}=0$. This expression shows that rectification due to electron-electron interaction appears for finite U and large E_r, even at

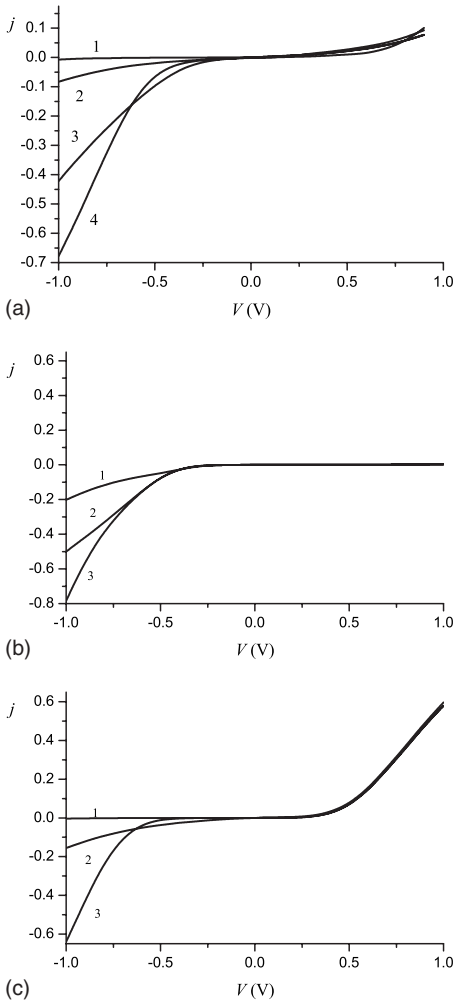

FIG. 5. Dependence of the tunneling current on the bias voltage to illustrate rectification. Condensed matter environment. The current normalized to $4ek^0$. Variable U_{eff}. $E_r=0.5$ eV, $\gamma=0.2$, and $k_BT=0.025$ eV. (a) $\eta=0$; (1) $U_{\mathrm{eff}}=-0.2$ eV, (2) $U=\infty$, (3) $U_{\mathrm{eff}}=0.1$ eV, (4) $U_{\mathrm{eff}}=0.2$ eV. (b) $\xi\eta=-0.2$ V; (1) $U_{\mathrm{eff}}=-0.2$ eV, (2) $U=\infty$, (3) $U_{\mathrm{eff}}=0.2$ eV. (c) $\xi\eta=0.2$ V; (1) $U=\infty$, (2) $U_{\mathrm{eff}}=0.2$ eV, (3) $U_{\mathrm{eff}}=0.5$ eV.

$\eta=0$, Fig. 5(a). The current is suppressed in the region $V<0$ and vice versa when $U_{\mathrm{eff}}<0$. Further, as an illustration, $r(0.5\text{ V},0)=3$ and $r(1\text{ V},0)=7$ at $U_{\mathrm{eff}}=0.2$ eV. Figure 5(b) shows that additional rectification appears for $\eta<0$, giving, e.g., $r(0.5\text{ V},-0.2\text{ V})=210$ and $r(1\text{ V},-0.2\text{ V})=230$ for $U_{\mathrm{eff}}=0.2$ eV. Figure 5(c) shows that the tunneling current is enhanced in the region $V<0$ even for $\eta>0$ compared with infinite U when $|U_{\mathrm{eff}}|<|(0.5-\gamma)eV|$. All the curves in Figs. 5(a)–5(c) tend to their asymptotic values $\pm ek^0(\pi E_r/k_BT)^{1/2}$ for $|V|>4$ V and finite U_{eff}.

VI. THE CURRENT/BIAS VOLTAGE DEPENDENCE AND THE DIFFERENTIAL CONDUCTANCE

One of the most important characteristics of the tunneling contact is the differential conductance $G=\partial j/\partial(eV)$. The $G(V)$ curves show much greater variety of features than the current/bias voltage correlations themselves and illustrate more precisely the physical nature of the rectification and other conductivity features. From Eq. (29),

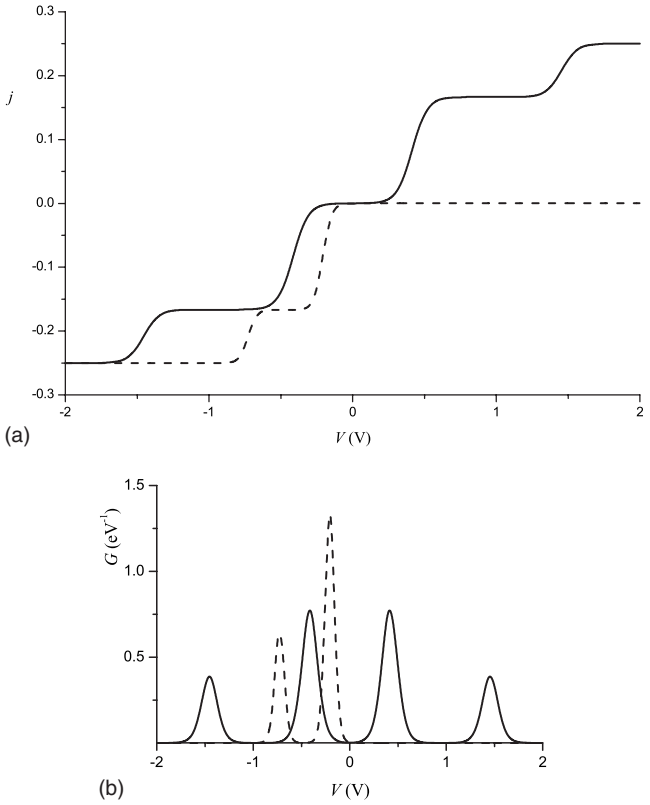

FIG. 6. Dependences of the tunneling current (a) and differential conductance $d(j/4ek^0)/d(eV)$ (b) on the bias voltage for the vacuum tunneling contact at $k_BT=0.025$ eV, $\eta_0=-0.2$ V, $U=0.5$ eV, $E_r=0$, and different γ. The current is normalized to $4eC^0$. Solid line: $\gamma=0.5$. Dashed line: $\gamma=0$.

$$G(V,e\xi\eta,U_{\text{eff}}) = G(-V,-e\xi\eta+U_{\text{eff}}+2k_BT\ln(2),U_{\text{eff}}). \tag{50}$$

Using Eqs. (30) and (31) and for $\gamma=0.5$ (vacuum tunneling),

$$G(V,\eta_0,U_{\text{eff}}) = G(-V,\eta_0,U_{\text{eff}}) \tag{51}$$

and

$$G(V,e\eta_0,U_{\text{eff}}) = G(V,-e\eta_0+U_{\text{eff}}+2k_BT\ln(2),U_{\text{eff}}). \tag{52}$$

Starting from vacuum tunneling we consider first the case when $|\varepsilon_{b0}|$, $|\varepsilon_{b0}+U| \gg k_BT$, and $E_r=0$. The peak positions of the differential conductance can be found using the expressions for the tunneling current but can also be obtained using an obvious physical consideration. Fixed bridge molecular levels are usually studied (i.e., $\gamma=0$). The tunneling current in this case starts to flow when the Fermi level of the right electrode (equal to $-eV$) reaches the ionization level of the bridge molecule. The position V_1 of the corresponding $G(V)$ peak equals $-\varepsilon_{b0}/e$ or η_0 with the accuracy of the order of k_BT. The position V_2 of the second peak of $G(V)$ associated with the Fermi level of the right electrode reaching the affinity level is at $-(\varepsilon_{b0}+U)/e$ or η_0-U/e. The case when $\gamma=0$ and $T \gg T_K$ [27,29,30] is shown by dashed curves in Fig. 6.

When the electric field in the tunneling gap is taken into account, $\gamma=0.5$ for the symmetric tunneling vacuum contact. Abrupt changes in the tunneling current then occur at *four* bias voltage values so that $G(V)$ has four peaks. The first value, V_1, is analogous to that considered above and corresponds to the Fermi level of the right electrode reaching the ionization level at $\varepsilon_{b0}-\gamma eV$: $V_1=-\varepsilon_{b0}/[e(1-\gamma)]=\eta_0/(1-\gamma)$. Also, $V_2=-(\varepsilon_{b0}+U)/[e(1-\gamma)]$ or $(\eta_0-U/e)/(1-\gamma)$. Since the ionization level is not fixed due to the change in the bias voltage, the third value, $V_{1\gamma}$, arises when the ionization level reaches the Fermi level of the left electrode so that $\varepsilon_{b0}-\gamma eV=0$, i.e., $V_{1\gamma}=\varepsilon_{b0}/(e\gamma)$ or $-\eta_0/\gamma$. Analogously, the fourth value, $V_{2\gamma}$, arises when the affinity level reaches the Fermi level of the left electrode: $V_{2\gamma}=(\varepsilon_{b0}+U)/(e\gamma)$ or $-(\eta_0-U/e)/\gamma$. We use the subscript γ at V in order to indicate that a given peak position of the $G(V)$ curve appears when γ is nonzero.

The case when $\varepsilon_{b0}=0.2$ eV and $\gamma=0.5$ is shown by solid curves in Fig. 6. The tunneling current is an odd function of V in this case, Eq. (30) and the differential conductivity an even function, Eq. (51). Figure 6(a) shows that $j(V)$ has the characteristic two-step structures in the regions $V<0$ and $V>0$. The first step in the region $V>0$ is two times higher than the second one.[30] The central peaks of the solid $G(V)$ curve in Fig. 6(b) are therefore twice the heights of the side peaks. It can be shown that the peak width at the points V_i are about $k_BT/[e(1-\gamma)]$ while the peak widths at $V_{i\gamma}$ are about $k_BT/(e\gamma)$. The peak widths for $\gamma=0$ [the dashed curve in Fig. 6(b)] is therefore half the widths of those for $\gamma=0.5$ [the solid curve in Fig. 6(b)].

It is well known[51] that the tunnel current can also be calculated using the spectral function[52] (or the electronic density of states) at the valence orbital of the redox molecule [see Eq. (C1)]. Electron-phonon interactions can be incorporated in the expressions for the $G(V)$ peaks analogously to those for V_i and $V_{i\gamma}$ obtained above by using the spectral functions A_o, A_1, A_{0a}, and A_2 defined in Appendix C and Eqs. (C1)–(C3). The differential conductance can have a number of peaks corresponding to the maxima E_o, E_1, E_{0a}, and E_2 of the spectral functions A_o, A_1, A_{0a}, and A_2. Particularly, if $|eV| \gg k_BT$, the term in the square brackets under the integral on the right hand side of Eq. (C1) can be omitted in the integration from $-eV$ to 0. Further, if the probabilities P_i vary slowly with the bias voltage, then the differential conductance is approximately a linear combination of the derivatives of the integrals of $A_\nu(\varepsilon)$ with respect to eV. Neglecting terms of order k_BT,

$$\frac{d}{d(eV)}\int_{-eV}^{0} A_\nu(\varepsilon)d\varepsilon = (1-\gamma)\exp\left[-\frac{(-eV-E_\nu)^2}{4E_rk_BT}\right] + \gamma\exp\left[-\frac{E_\nu^2}{4E_rk_BT}\right]. \tag{53}$$

Using the expressions for the energies E_ν, Appendix C, and Eq. (53) we obtain the following expressions for V_ν and $V_{\nu\gamma}$ of the $G(V)$ peaks:

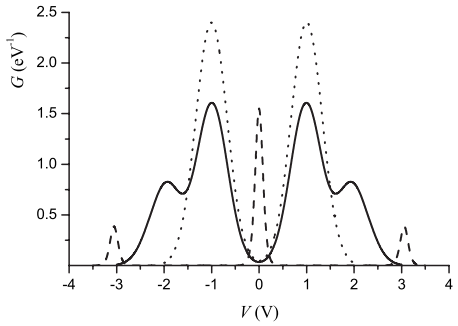

FIG. 7. Effect of E_r and U on the differential conductance $d(j/4ek^0)/d(eV)$ for the vacuum tunneling contact at $k_BT=0.025$ eV and $\gamma=0.5$. $\eta_0=0$. Solid line: $E_r=0.5$ eV, $U=1.5$ eV, $U_{eff}=0.5$ eV. Dashed line: $E_r=0$, $U=1.5$ eV. Dotted line: $E_r=0.5$ eV, $U=1$ eV, $U_{eff}=0$.

$$V_0=-\frac{E_r-e\xi\eta}{e(1-\gamma)},\quad V_{0\gamma}=\frac{E_r-e\xi\eta}{e\gamma},$$

$$V_1=\frac{E_r+e\xi\eta}{e(1-\gamma)},\quad V_{1\gamma}=-\frac{E_r+e\xi\eta}{e\gamma},$$

$$V_{0a}=-\frac{E_r-e\xi\eta+U_{eff}}{e(1-\gamma)},\quad V_{1a\gamma}=\frac{E_r-e\xi\eta+U_{eff}}{e\gamma},\tag{54}$$

$$V_2=\frac{E_r+e\xi\eta-U_{eff}}{e(1-\gamma)},\quad V_{2\gamma}=-\frac{E_r+e\xi\eta-U_{eff}}{e\gamma}.$$

It follows straightforwardly that the width at half maximum W_ν of the peaks centered at V_ν equals $4[E_rk_BT\ln(2)]^{1/2}/(1-\gamma)$ while $W_{\nu\gamma}=4[E_rk_BT\ln(2)]^{1/2}/\gamma$. The peaks at V_ν and $V_{\nu\gamma}$ appear in the differential conductivity with the weights $1-\gamma$ and γ, respectively, Eq. (53). Equation (54) also implies that the $G(V)$ curve may show up to eight peaks but some of them cannot be observed due to negligibly small P_i or strong overlap between the peaks. In the region $|eV|<E_r$ the probabilities P_i also vary rapidly with V, Eqs. (40) and (41), which shows that the characteristic energy scale of eV is k_BT in the limit of large E_r. The peaks in this region can therefore be altogether absent.

Incorporation of the electron-phonon interaction leads to additional peaks absent in vacuum tunneling contacts with $E_r=0$. When $\varepsilon_{b0}\approx 0$ and $E_r=0$, the tunneling current begins to flow when nonzero bias voltage is applied. The differential conductance has a peak at $V=0$ in this case (see dashed line in Fig. 7) and two Coulomb blockade peaks at $V_2=\pm U/e(1-\gamma)$ ($U=1.5$ eV in Fig. 7). When the electron-phonon interaction is taken into account, the central peak of the $G(V)$ curve splits into two peaks at $V_{0\gamma}=V_1=2E_r$ and $V_0=V_{1\gamma}=-2E_r$ (solid line in Fig. 7). The spectral functions $A_0(\varepsilon)$ and $A_1(\varepsilon)$ give the same contribution to both central peaks in this case. It follows from Eq. (40) that $P_o=P_1\approx 1/2$ and $P_2\approx 0$ for $\gamma=0.5$, $e\eta_0=0$, $U_{eff}=U-2E_r=0.5$ eV and $|eV|<E_r$. Since $V_2=V_{2\gamma}=0$, the spectral function A_2 gives no contribution to the differential conductance. However, P_1 varies slowly with increasing $|eV|$ so that $G(V)$ displays two Coulomb blockade peaks at $V_{0a\gamma}=|V_{0a}|=2(E_r+U_{eff})/e=2$ V. In accordance with Eq. (52), this curve also describes the case when $e\eta_0=U_{eff}+2k_BT\ln(2)$. If $U=1$ eV ($U_{eff}=0$), the Coulomb blockade peaks merge with the central peaks into two large central peaks (dotted line in Fig. 7).

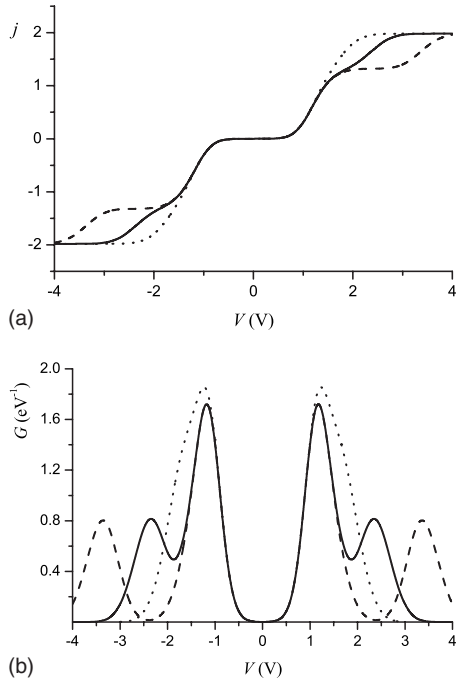

FIG. 8. Dependences of the tunneling current (a) and differential conductance $d(j/4ek^0)/d(eV)$ (b) on the bias voltage for the vacuum tunneling contact for and $k_BT=0.025$ eV, $E_r=0.5$ eV, $\eta_0=-0.2$ V, $\gamma=0.5$, and different values of U_{eff}. Solid line: $U_{eff}=0.5$ eV. Dashed line: $U_{eff}=1$ eV. Dotted line: $U_{eff}=0.2$ eV.

Figure 8 shows the current/bias voltage and the differential conductance/bias voltage dependencies for $\gamma=0.5$, $E_r=0.5$ eV, $\varepsilon_{b0}=0.2$ eV (or $e\eta_0\approx -0.2$ eV), and different values of U_{eff}. As for the case when $E_r=0$ [Fig. 6(a)], the dashed curve in Fig. 8(a) demonstrates the two-step structure where the first step in the region $V>0$ is twice higher than the second one. These steps merge into one for $U_{eff}=0.5$ and 0.8 eV [dotted and solid curves in Fig. 8(a)]. In accordance with Eq. (54), the $G(V)$ peaks for $U_{eff}=0.5$ eV are shifted by $\approx 2E_r$ and $\approx 2|e\eta_0|$ compared with the solid curves in Figs. 6(b) and 7, respectively. At the same time, when η_0 is nonzero, the physical nature of the central peaks in another than for $\eta_0=0$. From Eq. (40) $P_o\approx 1$ and $P_1\approx P_2\approx 0$ for $\eta_0\approx -0.2$ V and $|eV|<E_r$. Two central large peaks in Fig. 8(b) at $V_{0\gamma}=\pm|V_0|=2(E_r-e\eta_0)/e=1.4$ V for $U_{eff}=0.5$ eV and 1 eV are therefore due to the spectral function $A_0(\varepsilon)$. At sufficiently large $|V|$($|V|\geq 2$ V) the probability P_1 is almost at its limiting value ($\approx 1/2$) so that the Coulomb blockade peaks in Fig. 8(b) at $V_{0a\gamma}=\pm|V_{0a}|=2(E_r-e\eta_0+U_{eff})/e$ correspond to the spectral function $A_{0a}(\varepsilon)$. The Coulomb blockade peaks merge with the two central peaks for $U_{eff}=0.2$ eV. When $\eta_0\approx 0.2$ V, the Coulomb blockade peaks merge with the central peaks already at $U_{eff}=0.5$ eV. The central peaks are caused by the spectral function A_1 in this case. In accordance with Eq. (51), $G(V,\eta_0)=G(-V,\eta_0)$ for all curves shown in Fig. 8(b). As follows from Eq. (52), the $G(V)$ curve for $\eta_0=-0.2$ V and $U_{eff}=0.5$ eV coincides with that for $e\eta_0=0.7$ eV$+k_BT\ln(2)$ and $U_{eff}=0.5$ eV. However, in accor-

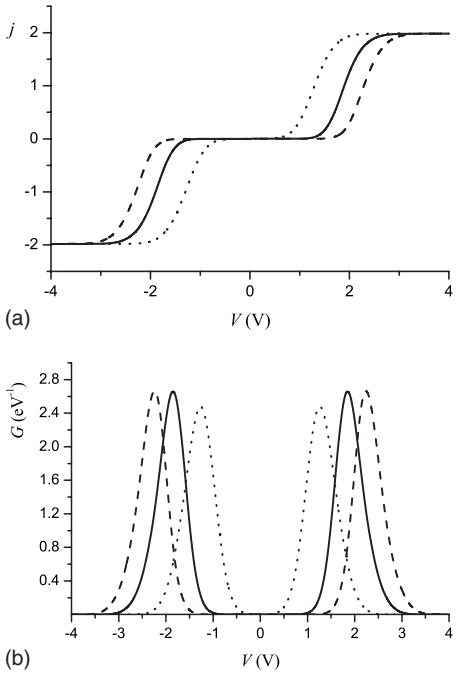

FIG. 9. Dependencies of the tunneling current (a) and differential conductance $d(j/4ek^0)/d(eV)$ (b) on the bias voltage for the vacuum tunneling contact for $\eta_0=-0.2$ V, $E_r=0.5$ eV, $\gamma=0.5$, and $k_BT=0.025$ eV. Negative U_{eff}. The current is normalized to $4ek^0$. Solid line: $U_{eff}=-0.8$ eV. Dashed line: $U_{eff}=-1$ eV. Dotted line: $U_{eff}=0$.

dance with Eq. (54), the physical nature of the peaks of the latter curve is different. In particular, the central peaks correspond to the spectral function A_2.

The current/bias voltage and differential conductance/bias voltage dependencies for $U_{eff}\leq 0$ are shown in Fig. 9. The nature of the $G(V)$ peaks for $U_{eff}=0$ [dotted line in Fig. 9(b)] is the same as for the peaks in Fig. 8(b). However, only the spectral function $A_2(\varepsilon)$ contributes to the differential conductance for $U_{eff}=-0.8$ eV and -1 eV because $P_2\approx 1$ and $P_0\approx P_1\approx 0$ for $|eV|<E_r$. The bridge molecular valence level in this case is in fact doubly occupied so that the current/bias voltage dependencies exhibit only a single step as for $U_{eff}=0$.

The correlations shown in Figs. 7–9 describe not only vacuum tunneling with interaction of the bridge molecular valence electron with intramolecular vibrations but also *in situ* tunneling with weak electric field screening by the solution. Intermediate screening ($\gamma=0.2$) is shown in Figs. 10 and 11. The simpler case is when $U\to\infty$ (Fig. 10). $P_0=P_1=1/2$ at $V=0$ when $\eta=0$. However, in contrast with the case when $\gamma=0.5$, P_1 decreases abruptly to negligibly small values when V increases from zero, Eq. (40). The right peak of the dotted line in Fig. 10 of width 0.37 eV/0.2 is therefore associated with the spectral function $A_0(\varepsilon)$ and lies at $V_{0\gamma}\approx E_r/0.2$. In contrast, P_0 decreases abruptly when V decreases from zero so that the left peak of the dotted curve is associated with the spectral function $A_1(\varepsilon)$ and lies at $V_{1\gamma}\approx -E_r/0.2$.

To illustrate, when $\xi\eta=0.2$ V (the dashed line in Fig. 10), $P_1=1$ at $V=0$. P_1 decreases slowly with increasing V whereas P_0 increases slowly so that both P_0 and P_1 vary slowly and have almost the same values at $V>1$ V. As a

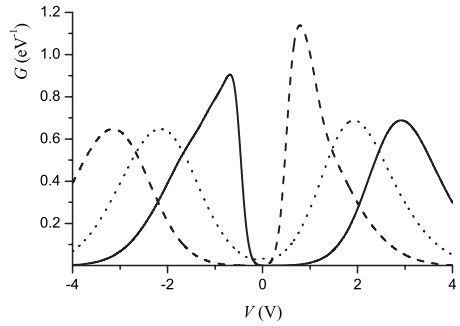

FIG. 10. Dependencies of the differential conductance $d(j/4ek^0)/d(eV)$ on the bias voltage in the infinite U limit for the *in situ* tunneling contact for $E_r=0.5$ eV, $\gamma=0.2$, and $k_BT=0.025$ eV. Solid line: $\xi\eta=-0.2$ V. Dashed line: $\xi\eta=0.2$ V. Dotted line: $\eta=0$.

result, the right peak of the dashed curve is composed of two peaks where the first peak is centered at $eV_1=(E_r+\xi\eta)/0.8\approx 0.9$ eV and a width proportional to $1/(1-\gamma)$. The second peak is centered at $eV_{0\gamma}=(E_r-\xi\eta)/0.2\approx 1.5$ eV and the width proportional to $1/\gamma$. Since $P_0\approx 0$ at $V=V_0$ whereas P_1 varies slowly from 1 to 2/3 in the region $V<0$, the left peak

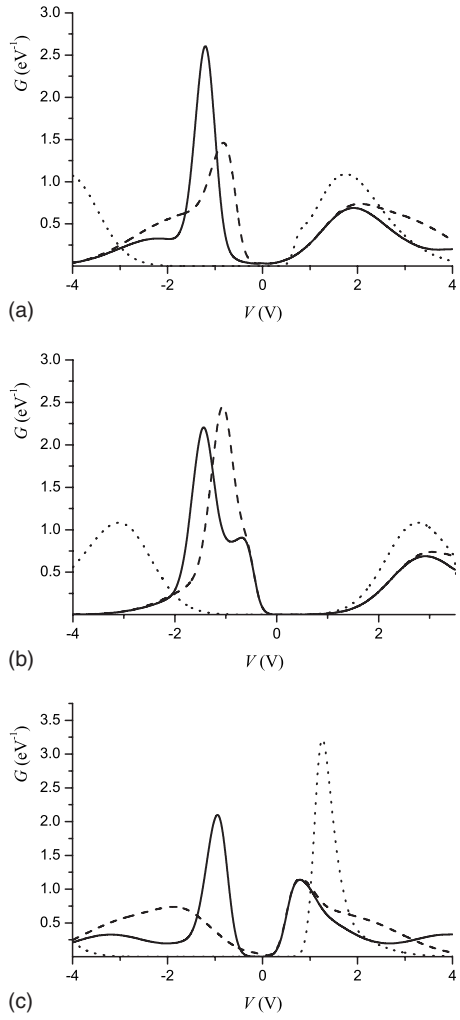

FIG. 11. Dependencies of the differential conductance $d(j/4ek^0)/d(eV)$ on the bias voltage for the *in situ* tunneling contact for $E_r=0.5$ eV, $\gamma=0.2$, and $k_BT=0.025$ eV. Finite U_{eff}. Solid line: $U_{eff}=0.5$ eV. Dashed line: $U_{eff}=0.2$ eV. Dotted line: $U_{eff}=-0.5$ eV. (a) $\eta=0$, (b) $\xi\eta=-0.2$ V, and (c) $\xi\eta=0.2$ V.

of the dashed curve in Fig. 10 is associated with the spectral function $A_1(\varepsilon)$ and centered at $eV_{1\gamma}=-(E_r+\xi\eta)/0.2\approx -3.5$ eV with the width proportional to $1/\gamma$.

When $\xi\eta=-0.2$ V (the solid curve in Fig. 10), the nature of the $G(V)$ peaks is opposite to those for $\xi\eta=0.2$ V. The right peak is centered at $V_{0\gamma}$ whereas the left peak is composed of two peaks where the first peak is centered at $eV_0=-(E_r-\xi\eta)/08\approx -0.9$ eV and the second one at $eV_{1\gamma}=-(E_r+\xi\eta)/0.2\approx -1.5$ eV. Figure 10 also shows that the approximate equality $G(V,\eta)=G(-V,-\eta)$ is fulfilled in the region of small V in the infinite-U limit.

Figure 10 also illustrates the physical meaning of the rectification effect shown in Fig. 4. For example, when $\xi\eta=-0.2$ V, the right $G(V)$ peak is shifted to the right proportionally to $|\xi\eta|/0.2$ compared with the case $\eta=0$ due to the Debye screening and negative η so that the current is negligibly small in the region $0\leq V<1$ V. In contrast, the $G(V)$ peak in the region $V<0$ is closer to $V=0$ than for $\eta=0$ (since it is also shifted to the right proportionally to $|\xi\eta|/0.2$) so that rectification arises. If screening is absent ($\gamma=0.5$) the left and right peaks are located symmetrically with respect to the axis $V=0$ even in the case $\xi\eta=-0.2$ V [the central peaks in Fig. 8(b)].

Figure 11 shows that compared with Fig. 10, additional Coulomb blockade peaks appear for finite positive U_{eff}. In contrast with the case shown in Fig. 8(b), Debye screening leads to a shift of the left Coulomb blockade peaks to the point $V=0$ ($V_{\text{oa}}(\gamma=0.5)/V_{\text{oa}}(\gamma=0.2)=1.6$) whereas the right Coulomb blockade peaks are shifted to the right from the center ($V_{\text{oa}\gamma}(\gamma=0.2)/V_{\text{oa}\gamma}(\gamma=0.5)=2.5$). The overpotential invokes an additional Coulomb blockade peak shift toward the center for $\eta>0$ and away from the center for $\eta<0$. As a result, the left Coulomb blockade peaks, Figs. 11(a) and 11(c), are closer to the center than those associated with the spectral function $A_1(\varepsilon)$ [compare Fig. 10 and Figs. 11(a)–11(c)]. Both peaks merge into a single feature for $U_{\text{eff}}=0.2$ eV with a left shoulder due to the contribution of the spectral function $A_1(\varepsilon)$. The Coulomb blockade peak lies to the left of the peak for $\xi\eta=-0.2$ V and $U_{\text{eff}}=0.5$ eV analogous to that shown in Fig. 10. The right Coulomb blockade peaks lie at $V_{\text{oa}\gamma}$ and are shown in Fig. 11(c) (at 2.5 and 4 V for $U_{\text{eff}}=0.2$ and 0.5 eV, respectively). These peaks are shifted by 1 and 2 V for $\eta=0$ and $\xi\eta=-0.2$ V, respectively, so that only the right shoulder is shown in the dashed curve in Fig. 11(a).

When Debye screening is taken into account, the differential conductance is no longer an even function of the bias voltage, Fig. 11. However, the validity of the identity given by Eq. (50) remains. For example, from Figs. 11(a) and 11(c) and for $U_{\text{eff}}=0.2$ eV, $G(V)$ at $\eta=0$ equals approximately $G(-V)$ at $\xi\eta=0.2$ V. Figure 11(a) and 11(b) also illustrate the physical meaning of the rectification in Figs. 5(a) and 5(b) while Fig. 11(c) explains the current/bias voltage curves in Fig. 5(c).

A clear peak at $V_2=1.5$ eV arising from the spectral function $A_2(\varepsilon)$ is seen in Fig. 11(c) when $U_{\text{eff}}=-0.5$ eV. Figures 11(a) and 11(b) show the left peaks also arising from the spectral function $A_2(\varepsilon)$ and located at the corresponding points $V_{2\gamma}$. However, the right peaks in $G(V)$ for $U_{\text{eff}}=-0.5$ eV and for $\eta=0$ and $\xi\eta=-0.2$ V are mainly due to the spectral function $A_0(\varepsilon)$ and are similar to those shown by dashed and solid lines. The right peak has a small left shoulder caused by the spectral function $A_2(\varepsilon)$ only for $\eta=0$.

VII. CONCLUSIONS

We studied the electric tunneling current/overpotential and tunneling current/bias voltage characteristics of a redox molecule with accessible oxidized and reduced redox levels in a tunneling gap between two enclosing metallic electrodes controlled by a common electrochemical reference or gate electrode. The system is representative of the working and tip electrode in electrochemical *in situ* scanning tunneling microscopy (STM) or of two electrodes in a nanogap electrochemical or solid state electronic device. Room temperature conditions and condensed matter environment are operating conditions. We specifically addressed the nonadiabatic limit of sequential tunneling of *two* electrons with (strong) Coulomb repulsion between the electrons that occupy the same energy level of the molecule, as well as strong electron-phonon interaction. The transfer of each electron in the overall two-ET step is thus controlled by configurational fluctuations in the solvent environment toward electronic resonance followed by full vibrational relaxation after each electronic transition. In addition to disclosing a range of novel electronic tunneling features specific to single-molecule two-electron, rather than single-electron tunneling, the system addressed is representative of electronic conductivity of redox molecules with three, instead of two electrochemically accessible oxidation states such as comprehensively reported.[1,3–14,16–20] The models addressed can be extended to multilevel transitions such as in the conductivity of molecular scale metallic nanoparticles and other molecular scale "quantum dots" with several closely spaced Coulomb-based single-electron levels.[24,26,53,54]

We have shown that even systems with a single redox level can display two clear peaks in the current/overpotential (gate voltage) dependence in the limit of strong electron-phonon interaction. One peak is the "intrinsic" redox peak, the other one the Coulomb peak. Unlike other reports on vacuum tunneling contacts,[28–30] the peaks are narrow (the width of the order of k_BT) due to the electron-phonon interaction and the appearance of a new energy scale, the reorganization (free) energy. As a result, the system exhibits two corresponding regions of tunneling current amplification. Approximate expressions for the peak positions and the critical value of the Coulomb repulsion determining the merging of the peaks into a single peak are obtained.

The amplification peaks in the tunneling current/overpotential (gate voltage) correlations are matched by tunneling spectroscopic features in the tunneling current/bias voltage or differential conductivity/bias voltage correlations. The former takes the form of a Coulomb staircase with four steps, the latter an equidistant four-peak sequence. The physical nature of the tunneling current steps or differential conductivity peaks differs from those in the tunneling current/overpotential amplification peaks (at small bias voltage). The bias voltage steps or peaks arise as successive ET

channels are opened when different electron or hole levels enter the energy window between the Fermi levels of the enclosing electrodes. The number of conducting channels thus increases with increasing bias voltage. Even though vibrational relaxation accompanies the electronic transitions, coherent electron or hole transport via all the levels continues as the bias voltage increases.

Coulomb repulsion between the electrons causes further rectification in the current/bias voltage dependence. For symmetric electronic coupling with the enclosing electrodes and symmetric redox molecule location in the tunneling gap, this effect is caused exclusively by the nonsymmetric position of the electronic redox energy level at fixed gate voltage for different signs of the bias voltage ($\gamma < 1/2$) due to the Debye screening.[21] Electrochemical tunneling contacts can therefore display single-molecule transistorlike behavior even for a single-level redox molecule.

Unlike studies where electron-phonon interaction was not included and the valence energy level considered as fixed,[28–30] the differential conductance/bias voltage correlations of single-level systems can finally have up to four peaks. These are associated with sequential electronic population of either the oxidized or reduced states of both the ionization and affinity levels of the redox molecule, equivalent to "push-pull" and "pull-push," or electron and hole transfer mechanisms forwarded and discussed elsewhere.[26,55] The peak positions are determined by the spectral function of both the ionization and affinity valence levels of the redox molecule.

The concepts and formalism introduced offers theoretical frames along several lines. The electronic conductivity of redox molecules with several, rather than only two redox states ("push-pull" and "pull-push" mechanisms via both ionization and affinity levels) offers first new mechanistic insight in fundamental two-electron (hole) transfer processes. The vibrational relaxation features of a single ET step in an overall multi-ET and multilevel process are thus subtle. The composite current/overpotential (gate voltage) and current/bias voltage correlations compared to single-ET with infinite electronic repulsion offers second prospects for design of more sophisticated molecular scale electronic working principles than for single-ET systems.

Experimental studies of sequential interfacial electrochemical ET and conductivity through redox molecules with several, well separated electronic redox states, at the level of the single molecule do not seem to be available presently. Several reported electrochemical *in situ* STM target molecular systems are, however, characterized by two successive electronic redox transitions. These are electrochemically accessible and some of the systems have shown strong *in situ* STM tunneling current/overpotential tunneling spectroscopic features but so far only with a single peak. The viologens and pyrrolotetrathiafulvalene are recent examples.[56–60] Oxidation of enclosing Au- or Pt-electrodes is probably prohibitive for the observation of both transitions but suitable choice of electrode and fine tuning of molecular structure may eventually resolve this issue. Other potential target systems include bipyridine- and terpyridine-based transition metal complexes of ruthenium, osmium, and perhaps other transition metal complexes stable in several oxidation states.[18,19,61,62] Os-complexes exhibit strong electrochemical tunneling spectroscopy[18,19] and are accessible in the II/III/IV oxidation states,[63] and might particularly offer such a class. Polynuclear cluster complexes of other transition metals (Fe, Mn, V, Mo) might hold other clues. Redox metalloproteins with several oxidation states such as ferredoxin/high-potential iron proteins[64] or multicenter redox metalloproteins and metalloenzymes could be still other contenders, although these system classes are at the limit of what *in situ* STM can cope with.[65,66]

Strong electronic coupling to intramolecular high-frequency nuclear modes similar to vibrational fine structure in optical transitions could be a new kind of target systems and have been addressed in low-temperature studies,[31–33] cf. above. Frequencies in excess of ≈ 1500 cm^{-1} would be needed for observation of vibrational fine structure in the condensed matter tunneling current/overpotential correlations at room temperature. This would bring focus on radical and atom transfer reactions but no such data are presently available.

Variable-size coated metallic and semiconductor, molecular scale nanoparticles ("quantum dots") may offer the best present prospects. These particles are characterized by sequences of electrochemically accessible electronic levels.[24–26] The spectral discreteness is caused both by the spatial confinement and successive Coulomb charging. The equally spaced level distribution is 150–180 mV for 1.5 nm Au_{145} coated nanoparticles[24–26] (corresponding to the size of polypyridine transition metal complexes). Only a single room temperature study of single-particle *in situ* STM of successive single-electron charging in aqueous electrolyte solution, and under electrochemical potential control, seems to have been reported.[26] This approach would, however, apply in general to metallic and semiconductor nanoparticles in the size range of 1–3 nm.

Condensed matter conductivity patterns of molecular scale nanoparticles show a complicated interplay between multiple electronic population and environmental nuclear relaxation.[26,67] This might, however, pay off by corresponding sophisticated electronic function in potential device contexts. Extension of the formalism offered presently can be a guide to the understanding of these phenomena.

ACKNOWLEDGMENTS

This work was partially supported by the Russian Foundation for Basic Research (Grant No. 09-03-00317a). J.U. acknowledges financial support from the Danish Research Council for Technology and Production Sciences (Grant No. 274-07-0272).

APPENDIX A: EXPRESSIONS FOR THE POSITIONS OF THE MINIMUM AND MAXIMA OF THE CURRENT/OVERPOTENTIAL DEPENDENCE

In this appendix we derive the expressions for the positions of the minima and maxima of the approximate current/

overpotential dependence given by Eq. (42) for the limit of large E_r. The right hand side of Eq. (42) is proportional to the function

$$\varphi(a,x) = \frac{2ax(a+x^2)}{x^4 + a^2(1+x^2)}, \tag{A1}$$

where $a = 2\exp(U_{\text{eff}}/2k_BT)$ and $x = \exp(e\eta_V/2k_BT)$. The derivative $d\varphi(a,x)/dx$ is proportional to

$$f(z) = z^3 + (3-a)z^2 - (3-a)z - 1, \tag{A2}$$

where $z = x^2/a$. The equation $f(z) = 0$ has the root $z = 1$ (or $x^2 = a$). The current/overpotential dependence therefore has an extremum at

$$\eta_V = (U_{\text{eff}}/2 + k_BT\ln(2))/e. \tag{A3}$$

It is readily shown that for $a > 6$ [or $U_{\text{eff}} > 2k_BT\ln(3)$], Eq. (A3) gives a minimum and for $a < 6$ [or $U_{\text{eff}} < 2k_BT\ln(3)$], a maximum of the current/overpotential dependence. It can also be shown that the equation $f(z)/(z-1) = z^2 - (a-4)z + 1$ has two positive roots,

$$z_{1,2} = 0.5\{a - 4 \pm [(a-4)^2 - 4]^{1/2}\}/2, \tag{A4}$$

only when $a > 6$. These roots correspond to the positions of maxima of the current/overpotential dependence. It can be shown that $z_1 \approx 1/a$ (or $x \approx 1$) and $z_2 \approx a$ (or $x \approx a$) for $a \gg 1$. The maxima of the current/overpotential dependence are then given by

$$\eta_V \approx 0, \quad \eta_V \approx U_{\text{eff}} + 2k_BT\ln(2). \tag{A5}$$

Since a equals ≈ 15 already for $U_{\text{eff}} = 0.1$ eV, Eq. (A5) is almost exact for all practically important cases. As a result, for $U_{\text{eff}} > U_{\text{eff}^*} = 2k_BT\ln(3) \approx 0.055$ eV, the current/overpotential dependence has two maxima and one minimum with positions given by Eqs. (A5) and (A3), respectively. For $U_{\text{eff}} < U_{\text{eff}^*}$, the current/overpotential dependence has only one maximum the position of which is given by Eq. (A3). We also note that, at $\eta_V = 0$, $\varphi(a,1) \approx 1$, 4/3, and ≈ 0 for $a \gg 1$, $U_{\text{eff}} = 0$, and $a \ll 1$, respectively. For $a > 6$, the tunneling currents at the maxima have therefore approximately the same values since also $\varphi(a,1) \approx 1$ for $a \gg 1$. Its values at the minimum are proportional to $\exp(-U_{\text{eff}}/4k_BT)$ in this case. The maximum value of the tunneling current is proportional to $\exp(U_{\text{eff}}/4k_BT)$ at $a \ll 1$, $U_{\text{eff}} < 0$.

APPENDIX B: THE TUNNELING CURRENT AND THE PROBABILITIES P_i IN THE LARGE-BIAS VOLTAGE LIMIT

We consider here the large-bias voltage limit. We start from finite U_{eff} and consider first the limit when $|\gamma eV|$ and $|(1-\gamma)eV| \gg E_r$, $||\xi\eta|$, U_{eff}, k_BT. Here $0 < \gamma \leq 1/2$. Equation (13) can be rewritten as[11]

$$k_{ij}^{\alpha} = k^{\alpha}\exp[-(E_r - \Delta F_{ji}^{\alpha})^2/4E_rk_BT] \times \int \frac{dx}{1+\exp(2x)}\exp[x(1 - \Delta F_{ji}^{\alpha}/E_r - k_BTx/E_r)]. \tag{B1}$$

The exponential factor in front of the integral represents the usual quadratic free energy form. Applying the saddle-point method for the evaluation of the integral I_{ij}^{α} in Eq. (B1), we obtain for $|\Delta F_{ji}^{\alpha}| \to \infty$,

$$I_{ij}^{\alpha} \approx (\pi E_r/k_BT)^{1/2}\exp[(E_r - |\Delta F_{ji}^{\alpha}|)^2/4E_rk_BT]. \tag{B2}$$

If $V \to \infty$, ΔF_{10}^{L} and ΔF_{21}^{L} tend to infinity whereas ΔF_{10}^{R} and ΔF_{21}^{R} tend to minus infinity. Using Eqs. (B1), (B2), and (14) we obtain

$$k_{01}^{L} \approx k_{10}^{R} \approx k_{12}^{L} \approx k_{21}^{R} \approx k^0\left(\frac{\pi E_r}{k_BT}\right)^{1/2}, \tag{B3}$$

and

$$k_{10}^{L} \approx k_{01}^{L}\exp(-\Delta F_{10}^{L}/k_BT), \quad k_{21}^{L} \approx k_{12}^{L}\exp(-\Delta F_{21}^{L}/k_BT), \tag{B4}$$

$$k_{01}^{R} \approx k_{10}^{R}\exp(-|\Delta F_{10}^{R}|/k_BT), \quad k_{12}^{R} \approx k_{21}^{R}\exp(-|\Delta F_{21}^{R}|/k_BT). \tag{B5}$$

As a result, the rate constants k_{01}^{L}, k_{10}^{R}, k_{12}^{L}, and k_{21}^{R} are finite and the rate constants k_{10}^{L}, k_{01}^{R}, k_{21}^{L}, and k_{12}^{R} infinitely small in the limit $V \to \infty$. Then, using Eq. (8) we obtain that the tunneling current tends to $ek^0(\pi E_r/k_BT)^{1/2}$ in this limit.

If $V \to -\infty$, the following approximate expressions for the rate constants are obtained that are opposite to Eqs. (B3)–(B5):

$$k_{10}^{L} \approx k_{01}^{R} \approx k_{21}^{L} \approx k_{12}^{R} \approx k^0\left(\frac{\pi E_r}{k_BT}\right)^{1/2}, \tag{B6}$$

and

$$k_{01}^{L} \approx k_{10}^{L}\exp(\Delta F_{10}^{L}/k_BT), \quad k_{12}^{L} \approx k_{21}^{L}\exp(\Delta F_{21}^{L}/k_BT), \tag{B7}$$

$$k_{10}^{R} \approx k_{01}^{R}\exp(-\Delta F_{10}^{R}/k_BT), \quad k_{21}^{R} \approx k_{12}^{R}\exp(-\Delta F_{21}^{R}/k_BT). \tag{B8}$$

The tunneling current thus tends to $-ek^0(\pi E_r/k_BT)^{1/2}$ in this limit.

Equations (B3)–(B8) show that the total rate constants $k_{ij} = k_{ij}^{L} + k_{ij}^{R}$ are finite and take the same value $k^0(\pi E_r/k_BT)^{1/2}$ in the limit $|V| \to \infty$. It is then readily obtained from Eq. (7) that $P_0 = P_2 \approx 1/4$ and $P_1 = 1/2$ in the limit $|V| \to \infty$ for both signs of the bias voltage.

Finally, we consider the infinite Coulomb repulsion limit, i.e., $U_{\text{eff}} \gg |eV|$, E_r, $|\xi\eta|$, k_BT. Then $\Delta F_{21}^{L(R)} \to -\infty$ so that $k_{12}^{L(R)} \to 0$ and $k_{21}^{L(R)} \to k^0(\pi E_r/k_BT)^{1/2}$. Using these expressions, we obtain Eqs. (9) and (10) from Eqs. (7) and (8). Considering next the large-bias voltage limit when $U_{\text{eff}} \gg |eV|$, i.e., $|\gamma eV|$ and $|(1-\gamma)eV| \gg E_r$, $||\xi\eta|$, k_BT, then Eqs. (B3)–(B8) remain valid for the rate constants with subscripts 01 and 10. We obtain therefore from Eq. (10) that the tunneling current tends to $\pm 2ek^0(\pi E_r/k_BT)^{1/2}/3$ in the limit $V \to \pm\infty$. The total rate constants k_{01} and k_{12} are also finite and

equal in the limit of infinite Coulomb repulsion so that we find from Eq. (9) that $P_0=1/3$ and $P_1=2/3$ in the limit $U_{\text{eff}} \gg |V| \to \infty$.

APPENDIX C: THE SPECTRAL FUNCTION AND THE TUNNELING CURRENT

The relation between the spectral function (or the electronic density of states) at the valence orbital of the redox molecule and the *in situ* tunneling current offers additional insight in the current/bias voltage dependence. The tunneling current can be calculated using[51]

$$j = \frac{2e\Delta^{\text{L}}\Delta^{\text{R}}}{\hbar\Delta}\int_{-\infty}^{\infty}[f_{\text{L}}(\varepsilon)-f_{\text{R}}(\varepsilon)]A(\varepsilon)\text{d}\varepsilon, \tag{C1}$$

where $A(\varepsilon)=\Sigma_\sigma A_\sigma(\varepsilon)$, $A_\sigma(\varepsilon)$ being the spectral function of the electron with spin projection σ at the valence level. Equation (C1) is valid both for weak and strong electronic-vibrational coupling. The factor in front of the integral is equal to $ek^0(\pi E_{\text{r}}/k_{\text{B}}T)^{1/2}/2$ for symmetric tunneling contacts and the limit of the nonadiabatic tunneling. In this limit the spectral function $A(\varepsilon)$ is a linear combination of the spectral functions $A_0(\varepsilon)$ and $A_1(\varepsilon)$ [see Eq. (20) of Ref. 12] for the spinless model or infinite-U limit where $A_0(\varepsilon)$ and $A_1(\varepsilon)$ are the spectral functions corresponding to the oxidized and reduced states of the redox molecule, respectively. Two new spectral functions $A_{0\text{a}}(\varepsilon)$ and $A_2(\varepsilon)$ should take into account finite U. $A_{0\text{a}}(\varepsilon)$ and $A_2(\varepsilon)$ are the spectral functions of the oxidized and reduced affinity level, respectively, corresponding to the electronic spin projection σ when the electron with spin projection $-\sigma$ already occupies the ionization level of the redox molecule. As a result,

$$A_\sigma(\varepsilon) = P_0A_0(\varepsilon) + P_\sigma A_1(\varepsilon) + P_{-\sigma}A_{0\text{a}}(\varepsilon) + P_2A_2(\varepsilon). \tag{C2}$$

The probabilities on the right hand side of Eq. (C2) are given by Eq. (7) in the weak-tunneling limit. The spectral functions $A_0(\varepsilon)$, $A_1(\varepsilon)$, $A_{0\text{a}}(\varepsilon)$, and $A_2(\varepsilon)$ are independent of k^0 for nonadiabatic tunneling and depend only on the electron-phonon and electron-electron interactions. The spectral function $A_0(\varepsilon)$ was obtained, e.g., in Ref. 52. The other spectral functions can also be obtained using the method of Ref. 52. These functions A_ν (ν=0, 1, 1a, and 2) normalized to unity have the form

$$A_\nu(\varepsilon) = (4\pi E_{\text{r}}k_{\text{B}}T)^{-1/2} \times\exp\{-[\varepsilon - E_\nu(E_{\text{r}},\varepsilon_{\text{b}},U_{\text{eff}})]^2/4E_{\text{r}}k_{\text{B}}T\}, \tag{C3}$$

with widths at half maximum of $4[E_{\text{r}}k_{\text{B}}T\ln(2)]^{1/2}$ ($\approx$0.37 eV for E_{r}=0.5 eV). Here $E_0=\varepsilon_{\text{b}}=-e\xi\eta-\gamma eV+k_{\text{B}}T\ln(2)+E_{\text{r}}$, $E_1=\varepsilon_{\text{b1}}=\varepsilon_{\text{b}}(q_{k\alpha})=\varepsilon_{\text{b}}-2E_{\text{r}}$, $E_{0\text{a}}=\varepsilon_{\text{b}}+U_{\text{eff}}$ and $E_2=\varepsilon_{\text{b}}+U_{\text{eff}}-2E_{\text{r}}$. The physical meaning of the electronic energy levels E_ν is as follows. E_{o} and $E_{0\text{a}}$ are the positions of the empty ionization and affinity levels, respectively. After thermal fluctuation of the vibrational subsystem and thermal fluctuation of the ionization (or affinity) level, the electron is transferred to the ionization (or affinity level if the ionization level is filled) followed by vibrational relaxation. As a result, the filled ionization or filled affinity levels are shifted by $-2E_{\text{r}}$ to E_1 or E_2. For the vacuum tunneling contact $E_0=\varepsilon_{\text{b0}}+E_{\text{r}}-\gamma eV=-e\eta_0-\gamma eV+k_{\text{B}}T\ln(2)+E_{\text{r}}$.

The physical meaning of the spectral functions $A_\nu(\varepsilon)$ follows from their integral representations:

$$A_0(\varepsilon) = \prod_k\left(\frac{\hbar\omega_k}{2\pi k_{\text{B}}T}\right)^{1/2}\int \text{d}q_k\delta\left(\varepsilon-\varepsilon_{\text{b}}+\sum_{k'}\gamma_{k'}q_{k'}\right) \times\exp\left(-\frac{\hbar\omega_k q_k^2}{2k_{\text{B}}T}\right). \tag{C4}$$

The fluctuations of the ionization level in the spectral function of the oxidized state of the redox molecule are thus averaged over the Boltzmann distribution for the coordinates of the free phonon modes in the absence of electron-phonon interactions. On the other hand,

$$A_1(\varepsilon) = \prod_k\left(\frac{\hbar\omega_k}{2\pi k_{\text{B}}T}\right)^{1/2}\int \text{d}q_k\delta\left(\varepsilon-\varepsilon_{\text{b}}+\sum_{k'}\gamma_{k'}q_{k'}\right) \times\exp\left[-\frac{\hbar\omega_k(q_k-q_{k\alpha})^2}{2k_{\text{B}}T}\right]. \tag{C5}$$

The fluctuations of the energy of the ionization level in the spectral function of the reduced state of the redox molecule are thus averaged over the Boltzmann distribution of the coordinates of the perturbed phonon modes with equilibrium values of q_k equal to $q_{k\alpha}$.

$A_{0\text{a}}(\varepsilon)$ and $A_2(\varepsilon)$ can be represented as, cf. the discussion above:

$$A_{0\text{a}}(\varepsilon) = \prod_k\left(\frac{\hbar\omega_k}{2\pi k_B T}\right)^{1/2}\int \text{d}q_k\delta\left(\varepsilon-\varepsilon_{\text{b}}-U+\sum_{k'}\gamma_{k'}q_{k'}\right) \times\exp\left[-\frac{\hbar\omega_k(q_k-q_{k\alpha})^2}{2k_{\text{B}}T}\right], \tag{C6}$$

$$A_2(\varepsilon) = \prod_k\left(\frac{\hbar\omega_k}{2\pi k_{\text{B}}T}\right)^{1/2}\int \text{d}q_k\delta\left(\varepsilon-\varepsilon_{\text{b}}-U+\sum_{k'}\gamma_{k'}q_{k'}\right) \times\exp\left[-\frac{\hbar\omega_k(q_k-2q_{k\alpha})^2}{2k_{\text{B}}T}\right]. \tag{C7}$$

Using Eqs. (22) and (40) for ε_{b} and P_i and taking the limit of large E_{r} in Eqs. (C1)–(C3), we obtain Eq. (42) as expected. When $|V|\to\infty$, the integral on the right hand side of Eq. (C1) is equal to $\pm(2P_{0\infty}+P_{1\infty})ek^0(\pi E_{\text{r}}/k_{\text{B}}T)^{1/2}/2 = \pm 2ek^0(\pi E_{\text{r}}/k_{\text{B}}T)^{1/2}/3$ in the infinite U limit and $\pm 2(P_0+P_1+P_2)ek^0(\pi E_{\text{r}}/k_{\text{B}}T)^{1/2}/2 = \pm ek^0(\pi E_{\text{r}}/k_{\text{B}}T)^{1/2}$ for finite U_{eff}. This coincides with the results in Appendix B.

[1] A. M. Kuznetsov and J. Ulstrup, Probe Microsc. **2**, 187 (2001).
[2] M. Galperin, M. A. Ratner, and A. Nitzan, J. Phys.: Condens. Matter **19**, 103201 (2007).
[3] J. Zhang, A. M. Kuznetsov, I. G. Medvedev, Q. Chi, T. Albrecht, P. S. Jensen, and J. Ulstrup, Chem. Rev. (Washington, D.C.) **108**, 2737 (2008).
[4] A. M. Kuznetsov, P. Sommer-Larsen, and J. Ulstrup, Surf. Sci. **275**, 52 (1992).
[5] W. Schmickler, Surf. Sci. **295**, 43 (1993).
[6] H. Sumi, J. Phys. Chem. B **102**, 1833 (1998).
[7] A. M. Kuznetsov and J. Ulstrup, J. Phys. Chem. A **104**, 11531 (2000).
[8] A. M. Kuznetsov and W. Schmickler, Chem. Phys. **282**, 371 (2002).
[9] I. G. Medvedev, J. Electroanal. Chem. **600**, 151 (2007).
[10] A. M. Kuznetsov and I. G. Medvedev, Electrochem. Commun. **9**, 1343 (2007).

[11] A. M. Kuznetsov, I. G. Medvedev, and J. Ulstrup, J. Chem. Phys. **127**, 104708 (2007).
[12] I. G. Medvedev, Phys. Rev. B **76**, 125312 (2007).
[13] I. G. Medvedev, Electrochim. Acta **53**, 6545 (2008).
[14] N. G. Tao, Phys. Rev. Lett. **76**, 4066 (1996).
[15] W. H. Han, E. N. Durantini, A. L. Moore, D. Gust, P. Rez, G. Leatherman, G. R. Seely, N. J. Tao, and S. M. Lindsay, J. Phys. Chem. B **101**, 10719 (1997).
[16] Z. Li, B. Han, G. Meszaros, I. Pobelov, Th. Wandlowski, A. Blaszczyk, and M. Mayor, Faraday Discuss. **131**, 121 (2006).
[17] Q. Chi, J.-D. Zhang, P. S. Jensen, H. E. M. Christensen, and J. Ulstrup, Faraday Discuss. **131**, 181 (2006).
[18] T. Albrecht, K. Moth-Poulsen, J. B. Christensen, A. Guckian, T. Bjornholm, J. G. Vos, and J. Ulstrup, Faraday Discuss. **131**, 265 (2006).
[19] T. Albrecht, A. Guckian, A. M. Kuznetsov, J. G. Vos, and J. Ulstrup, J. Am. Chem. Soc. **128**, 17132 (2006).
[20] A. Alessandrini, S. Corni, and P. Facci, Phys. Chem. Chem. Phys. **8**, 4383 (2006).
[21] A. A. Kornyshev, A. M. Kuznetsov, and J. Ulstrup, Proc. Natl. Acad. Sci. U.S.A. **103**, 6799 (2006).
[22] C. Joachim and M. A. Ratner, Proc. Natl. Acad. Sci. U.S.A. **102**, 8801 (2005).
[23] T. K. Ng and P. A. Lee, Phys. Rev. Lett. **61**, 1768 (1988).
[24] A. C. Templeton, W. P. Wuelfing, and R. W. Murray, Acc. Chem. Res. **33**, 27 (2000).
[25] B. M. Quinn, P. Liljeroth, V. Ruiz, T. Laaksonen, and K. Kontturi, J. Am. Chem. Soc. **125**, 6644 (2003).
[26] T. Albrecht, S. F. L. Mertens, and J. Ulstrup, J. Am. Chem. Soc. **129**, 9162 (2007).
[27] L. Y. Chen and C. S. Ting, Phys. Rev. B **44**, 5916 (1991).
[28] D. V. Averin, A. N. Korotkov, and K. K. Likharev, Phys. Rev. B **44**, 6199 (1991).
[29] A. L. Yeyati, A. Martin-Rodero, and F. Flores, Phys. Rev. Lett. **71**, 2991 (1993).
[30] B. Muralidharan, A. W. Ghosh, and S. Datta, Phys. Rev. B **73**, 155410 (2006).
[31] X. Li, H. Chen, and S.-x. Zhow, Phys. Rev. B **52**, 12202 (1995).
[32] E. G. Petrov, V. May, and P. Hänggi, Phys. Rev. B **73**, 045408 (2006).
[33] E. G. Petrov, Chem. Phys. **326**, 151 (2006).
[34] P. S. Cornaglia, H. Ness, and D. R. Grempel, Phys. Rev. Lett. **93**, 147201 (2004).
[35] D. Boese and H. Schoeller, Europhys. Lett. **54**, 668 (2001).
[36] S. Braig and K. Flensberg, Phys. Rev. B **68**, 205324 (2003).
[37] K. D. McCarthy, N. Prokof'ev, and M. T. Tuominen, Phys. Rev. B **67**, 245415 (2003).
[38] A. Mitra, I. Aleiner, and A. J. Millis, Phys. Rev. B **69**, 245302 (2004).
[39] J. Koch and F. von Oppen, Phys. Rev. Lett. **94**, 206804 (2005).
[40] A. M. Kuznetsov and I. G. Medvedev, Electrochem. Commun. **10**, 1191 (2008).
[41] A. M. Kuznetsov and I. G. Medvedev, Phys. Rev. B **78**, 153403 (2008).
[42] A. M. Kuznetsov, I. G. Medvedev, and V. V. Sokolov, J. Chem. Phys. **120**, 7616 (2004).
[43] A. M. Kuznetsov, *Charge Transfer in Physics, Chemistry and Biology* (Gordon & Breach, Reading, 1995).
[44] A. M. Kuznetsov and J. Ulstrup, *Electron Transfer in Chemistry and Biology: An Introduction to the Theory* (Wiley, Chichester, 1999).
[45] J. Koch, E. Sela, Y. Oreg, and F. von Oppen, Phys. Rev. B **75**, 195402 (2007).
[46] A. Aviram and M. A. Ratner, Chem. Phys. Lett. **29**, 277 (1974).
[47] R. Stadler, V. Geskin, and J. Copnil, J. Phys.: Condens. Matter **20**, 374105 (2008).
[48] A. M. Kuznetsov and J. Ulstrup, J. Chem. Phys. **116**, 2149 (2002).
[49] R. Metzger, Chem. Rev. (Washington, D.C.) **103**, 3803 (2003).
[50] F. Zahid, A. W. Ghosh, M. Paulson, E. Polizzi, and S. Datta, Phys. Rev. B **70**, 245317 (2004).
[51] Y. Meir and N. S. Wingreen, Phys. Rev. Lett. **68**, 2512 (1992).
[52] C. D. Mahan, *Many Particle Physics* (Plenum, New York, 1990).
[53] R. P. Andres, T. Bein, M. Dorogi, S. Feng, J. I. Henderson, C. P. Kubiak, W. Mahoney, R. G. Osifchin, and R. Reifenberger, Science **272**, 1323 (1996).
[54] A. G. Hansen, H. Wackerbarth, J. U. Nielsen, J. Zhang, A. M. Kuznetsov, and J. Ulstrup, Russ. J. Electrochem. **39**, 108 (2003).
[55] R. R. Dogonadze, J. Ulstrup, and Yu. I. Kharkats, J. Theor. Biol. **40**, 259 (1973).
[56] W. Haiss, R. J. Nichols, H. van Zalinge, S. Higgins, D. Bethell, and D. J. Schiffrin, J. Am. Chem. Soc. **125**, 15294 (2003); Phys. Chem. Chem. Phys. **6**, 4330 (2004).
[57] W. Haiss, R. J. Nichols, H. van Zalinge, S. Higgins, D. Bethell, and D. J. Schiffrin, Langmuir **20**, 7694 (2004).
[58] I. V. Pobelov, Z. Li, and T. Wandlowski, J. Am. Chem. Soc. **130**, 16045 (2008).
[59] W. Haiss, T. Albrecht, H. van Zalinge, S. J. Higgins, D. Bethell, H. Höhenreich, D. J. Schiffrin, R. J. Nichols, A. M. Kuznetsov, J. Zhang, Q. Chi, and J. Ulstrup, J. Phys. Chem. B **111**, 6703 (2007).
[60] E. Leary, S. J. Higgins, H. van Zalinge, W. Haiss, R. J. Nichols, S. Nygaard, J. O. Jeppesen, and J. Ulstrup, J. Am. Chem. Soc. **130**, 12204 (2008).
[61] D. Natelson, L. H. Yu, J. W. Ciszek, Z. K. Keane, and J. M. Tour, Chem. Phys. **324**, 267 (2006).
[62] B. R. Crane, A. J. Di Bilio, J. R. Winkler, and H. B. Gray, J. Am. Chem. Soc. **123**, 11623 (2001).
[63] T. J. Meyer and M. H. V. Huynh, Inorg. Chem. **42**, 8140 (2003).
[64] J. Zhang, H. E. M. Christensen, B. L. Ooi, and J. Ulstrup, Langmuir **20**, 10200 (2004).
[65] J. Zhang, A. C. Welinder, H. E. M. Christensen, and J. Ulstrup, J. Phys. Chem. B **107**, 12480 (2003).
[66] J. D. Gwyer, J. Zhang, J. N. Butt, and J. Ulstrup, Biophys. J. **91**, 3897 (2006).
[67] A. M. Kuznetsov and J. Ulstrup, J. Electroanal. Chem. **564**, 209 (2004).